NACA RM L57E16

NACA

RESEARCH MEMORANDUM

INVESTIGATION AT TRANSONIC SPEEDS OF THE EFFECTS OF INLET-LIP SWEEP ON THE INTERNAL-FLOW CHARACTERISTICS OF A SEMIELLIPTICAL AIR INLET WITH AN INLET-LIP STAGGER OF 30°

By Charles D. Trescot, Jr.

Langley Aeronautical Laboratory
Langley Field, Va.

NATIONAL ADVISORY COMMITTEE FOR AERONAUTICS

WASHINGTON

July 23, 1957
Declassified September 29, 1959

NATIONAL ADVISORY COMMITTEE FOR AERONAUTICS

RESEARCH MEMORANDUM

INVESTIGATION AT TRANSONIC SPEEDS OF THE EFFECTS OF INLET-LIP SWEEP ON THE INTERNAL-FLOW CHARACTERISTICS OF A SEMIELLIPTICAL AIR INLET WITH AN INLET-LIP STAGGER OF 30°

By Charles D. Trescot, Jr.

SUMMARY

An investigation has been conducted in the Langley transonic blowdown tunnel to study the effects of inlet-lip sweep angle on the internal-flow characteristics of a semielliptical scoop-type inlet with an inlet-lip stagger of 30°. The inlet sweep angle was varied from 45° sweepforward to 45° sweepback in increments of 15°. Tests were made at Mach numbers of 1.0, 1.2, and 1.4 through a mass-flow ratio range of about 0.4 to 0.9 at an angle of attack of 0°.

The test results indicate that the average total-pressure recovery and flow distortions of the sweptforward inlets were superior to those of the sweptback inlets at all test conditions. Increases in inlet sweepforward angle produced improvements in both pressure recovery and flow distortions at the high mass-flow ratios when compared with an unswept inlet whereas increases in inlet sweepback always produced adverse effects on the pressure recovery and flow distortions. The advantages of the sweptforward inlets were attributed largely to a natural bypassing of the fuselage boundary layer. A simple slot cut in the lips of the 45° sweptback inlet improved the pressure recovery and flow distortions of this inlet equally as well as a boundary-layer diverter of the same height.

INTRODUCTION

Normal-shock pressure recovery has been obtained in some instances (ref. 1) for round-lip fuselage scoop-type inlets at Mach numbers to 1.4 without benefit of boundary-layer-control devices. As described in reference 1, a natural bypassing action of the boundary layer permitted

attainment of these high values of pressure recovery on an unswept inlet with 30° of lip stagger, even though a thickened or separated boundary layer existed ahead of the inlet because of the inlet terminal shock. On the other hand, an inlet having a lip stagger of 30°, but sweptback 45°, apparently did not bypass significant quantities of boundary layer with the result that the internal performance of this inlet was lower than that of the unswept inlet. Consequently, a program of investigation to study the effect of inlet-lip stagger and sweep on the natural bypassing phenomena was undertaken. Results of tests of an unswept semi-elliptical inlet with lip stagger varying from 0° to 60° (ref. 2) show that the optimum stagger angle for maximum boundary-layer bypassing and maximum total-pressure recovery of an unswept inlet was of the order of 30°.

This paper presents the results of an investigation to determine the effect of inlet sweep on boundary-layer bypassing. For this investigation, the inlet sweep was varied from 45° sweepforward to 45° sweepback in increments of 15°. Based upon the results of reference 2, an inlet-lip stagger of 30° was used throughout the investigation. The tests were made in the Langley transonic blowdown tunnel at Mach numbers of 1.0, 1.2, and 1.4 through a mass-flow-ratio range of about 0.4 to 0.9 at an angle of attack of 0°.

SYMBOLS

p_t	total pressure
p	static pressure
$\frac{p_{t,i} - p_\infty}{p_{t,\infty} - p_\infty}$	impact-pressure ratio
$\frac{p - p_\infty}{p_{t,\infty} - p_\infty}$	static-pressure ratio
$\frac{\bar{p}_{t,i}}{p_{t,\infty}}$	average inlet total-pressure recovery weighted with respect to mass flow, $\frac{\int_A \frac{\rho V}{\rho_\infty V_\infty} \frac{p_{t,i}}{p_{t,\infty}} dA}{\int_A \frac{\rho V}{\rho_\infty V_\infty} dA}$

$\frac{p_{t,i,max} - p_{t,i,min}}{\bar{p}_{t,i}}$	total distortion parameter, defined as the ratio of maximum inlet total-pressure difference to integrated inlet total-pressure recovery
$\frac{w_i}{w_\infty}$	mass-flow ratio, defined as ratio of total inlet mass flow to mass flow through a free-stream tube with area equal to that of minimum projected frontal area of inlet (0.556 sq in.)
w	rate of mass flow
M	Mach number
V	velocity
D	diameter
A	duct area
ρ	mass density, slugs/cu ft
Λ	inlet sweep angle, positive when sweptback and negative when sweptforward

Subscripts:

i	inlet
∞	free stream
max	maximum
min	minimum

MODEL

A photograph of the model is presented in figure 1 and a sketch of the model is shown in figure 2. The model, comparable to that employed for the stagger investigation (ref. 2), consisted of a semielliptical scoop-type inlet (see table I) mounted on a body of revolution. The nose of the body was 4.67 inches long and was formed by rotating NACA 1-series nose-inlet coordinates about the center line with a radius of 1 inch at the maximum diameter. (See table I.) Behind fuselage station 4.67, the body was cylindrical. The inlet was symmetrical about the vertical center

line and the ratio of maximum height to maximum width was 1.5. The inlet lips were approximately semielliptical in shape and had a length-to-thickness ratio of 2.0. The ratio of the minimum projected frontal area of the inlet to the maximum frontal area of the fuselage alone was 0.177.

During the course of the investigation, the inlet sweep angle was varied from 45° sweepforward to 45° sweepback in increments of 15°. The center line of the inlet in the vertical plane always intersected the fuselage at station 5.85 irrespective of inlet sweep angle. (See fig. 2.) A lip stagger of 30° was incorporated for all configurations.

The area distribution of the internal ducting (exclusive of instrumentation) is shown in figure 3. From the inlet plane back to the inlet measuring station, the duct area was constant. Behind this station, the side walls diverged at a rate equivalent to that of a 6° conical diffuser and faired into a rectangular duct at station 13.25. The inlet mass-flow ratio was measured at a rectangular-shaped venturi located at fuselage station 14.62 and was controlled by varying the area at the exit of the duct.

APPARATUS AND METHODS

Pressure Measurements

The pressure instrumentation at the inlet and venturi measuring station is shown in figure 2. The inlet measuring station instrumentation included 20 total-pressure tubes and 1 static-pressure tube located at station 8.00 and 1 surface orifice located at fuselage station 7.80. The venturi measuring station instrumentation included 25 total-pressure tubes, 2 static-pressure tubes, and 1 surface orifice. Static-pressure orifices were distributed along the vertical center line of the fuselage and extended from station 1.00 on the nose to the inlet measuring station.

Flow Study

Schlieren photographs and oil-flow studies were used to aid in the study of the nature of the flow ahead of the inlet measuring station. The patterns made by the oil droplets, which were placed in and around the inlet, were photographed after each run. The photographs of the oil-flow traces indicated the direction of the flow within the boundary layer.

Tests

The tests were conducted in the Langley transonic blowdown tunnel at Mach numbers of 1.0, 1.2, and 1.4 through a mass-flow-ratio range of about 0.4 to 0.9 at an angle of attack of 0°. The tunnel stagnation pressure was held constant at either 53 pounds per square inch absolute or 60 pounds per square inch absolute with a resulting Reynolds number range of about 2.9×10^6 to 3.3×10^6 based on the body diameter of 2 inches. An encircling roughness band was put on the nose to insure that the boundary-layer flow reaching the inlet would be turbulent. This band extended from fuselage station 0.5 inch to 0.75 inch and consisted of 0.003- to 0.005-inch-diameter grains of carborundum on a thin layer of shellac. The estimated accuracy of the test data is as follows:

$$\frac{p_{t,i} - p_\infty}{p_{t,\infty} - p_\infty} \quad \pm 0.005$$

$$\frac{\bar{p}_{t,i}}{p_{t,\infty}} \quad \pm 0.01$$

$$\frac{w_i}{w_\infty} \quad \pm 0.02$$

RESULTS AND DISCUSSION

Flow Over the Nose

The static-pressure distributions (fig. 4) indicate that local Mach numbers greater than free-stream values existed over the fuselage nose for every test condition. For example, local Mach numbers of about 1.15 and 1.48 were indicated for free-stream Mach numbers of 1.0 and 1.4, respectively. The supersonic flow ahead of the inlet terminated in a shock wave for all test conditions as indicated by the abrupt compression ahead of the inlets. For free-stream Mach numbers of about 1.2 and above, schlieren photographs of the flow about the various inlets (fig. 5) showed that the inlet compression was in the form of a λ-type shock rather than the normal shock that occurred at the highest mass-flow ratio at $M = 1.0$. At this Mach number, a tendency towards the formation of a λ-type shock also occurred as the mass-flow ratio was decreased. Inasmuch as a transition strip was located well forward on the fuselage nose to assure a turbulent boundary layer, a λ-type shock formation must be associated with turbulent separation, as pointed out in reference 3.

The initial static-pressure rise ahead of the inlet indicates the position of the front leg of the λ-shock. It can be seen in figure 4 that the inlet shock moves rearward as the inlet sweep angle is varied from 45° sweepforward to 45° sweepback. It also appears that the compression of the flow entering the inlet which is needed to satisfy the inlet mass-flow requirements is accomplished ahead of the inlet-lip-fuselage juncture in the case of the sweptforward inlets but persists into the inlet for the sweptback inlet configurations.

Total-Pressure Recovery at Inlet

The average total-pressure recovery for the several sweptforward and sweptback inlet configurations is presented in figures 6(a) and (b), respectively, as a function of inlet mass-flow ratio for the test Mach number range.

Sweptforward inlets.- The total-pressure recoveries for all sweptforward configurations approached 1.0 at the lower mass-flow ratios for a Mach number of 1.0, the values decreasing slightly with increasing mass-flow ratio. Increases in test Mach number resulted in lower total-pressure recoveries as a result of shock and shock-boundary-layer interaction effects, as will be discussed later. It is interesting to note, however, that the highest recovery obtained at a Mach number of 1.4 was only about 1 percent lower than that across a normal shock $\left(\frac{\bar{p}_t}{p_{t,\infty}} = 0.96\right)$; thus, losses resulting from shock—boundary-layer interaction effects were not large for this case.

Increases in inlet sweep angle from 0° to -45° had a negligible effect on the average recovery at Mach numbers of 1.0 and 1.2 for the full range of test mass-flow ratio. The largest differences were obtained at a Mach number of 1.4 for a mass-flow ratio of 0.9. Here, the 15° and 30° sweptforward inlets had recoveries about 2 to 3 percent greater than that for the unswept inlet. Although the differences in total-pressure recovery between the various configurations are not large, the aerodynamics of the flow processes are very different and will be discussed briefly.

Schlieren photographs of the flow about the various inlets (fig. 5) show that, in every case, separation existed ahead of the inlet at Mach numbers above about 1.2. The fact that no evidence of flow separation was obtained at the inlet measuring station (figs. 7(a) to 7(d)) indicates that a boundary-layer-bypassing action similar to that discussed in references 1 and 2 occurred for all configurations. These references point out that, when the inlet terminal shock is located at some distance ahead of the inlet, thickened or separated boundary layer can bleed around the inlet lips provided a sufficient pressure differential exists between the internal and external flow. Some boundary-layer-bypassing

action is shown to have occurred for all inlets by the oil-flow photographs of figure 8. These photographs show that in every case some of the flow next to the fuselage surface actually entered the inlet, then reversed direction, and escaped around the inlet lips.

Examination of the inlet impact-pressure-ratio contours of figures 7(a) to 7(d) will show a marked improvement in total pressure immediately adjacent to the fuselage surface as the inlet sweep angle was increased from 0° to -45°. This increase in local recovery was the origin of the 2- to 3-percent increase in average total-pressure recovery at a Mach number of 1.4 shown for the -15° and -30° inlets in figure 6(a). It is believed that an increasing amount of flow bypassing with increasing sweep forward was responsible for the improved local pressure recovery. These increases in the amount of bypassed flow for the present configuration are attributed largely to the shock location rather than to differences in pressure differential inasmuch as the static pressures for all inlets were nearly the same at comparable values of mass-flow ratio. Measurements of the shock location from the schlieren photographs (fig. 5) and the static-pressure distributions over the nose (fig. 4(b)) show a definite increase in distance between the most forward leg of the shock and the inlet-lip—fuselage juncture station with an increase in forward sweep. The oil-flow traces, of course, do not indicate the quantities of flow being bypassed around the inlets, but close examination of figures 8(a) and 8(b) will show that the number and intensity of the traces moving around the inlets definitely increased with increasing forward sweep.

Although this bypassing action continued to increase up to the maximum sweep angle of the present tests, the average total-pressure recovery of the 45° sweptforward inlet was slightly lower than that for the -15° and -30° inlets. The small decrease in recovery shown in figure 6(a) for the 45° sweptforward inlet is believed to result from a change in inlet shock formation. At a Mach number of 1.4, schlieren photographs (fig. 5(a)) show that a secondary shock, probably resulting from an overexpansion of flow around the inlet lip, occurred in the outboard end of the inlet for mass-flow ratios of 0.69 and above. The interaction of this shock with the main inlet shock generated a vortex that entered the inlet and produced the two plateaus of equal impact-pressure ratio shown by the contours in figure 7(a).

Sweptback inlets.- As was the case for the sweptforward inlets, the total-pressure recovery of the sweptback inlets decreased with increases in test Mach number (fig. 6(b)). Unlike the sweptforward inlets, however, increases in inlet sweepback angle from 0° to 45° effected appreciable decreases in the average total-pressure recovery at all test Mach numbers. In addition, reductions in mass-flow ratio generally produced a decrease in the average total-pressure recovery for the sweptback inlets.

Examination of the impact-pressure-ratio contours (figs. 7(e) to 7(g)) shows that, although the maximum measured values of total pressure approach the stream value in the outboard end of the inlets, a region of total-pressure loss which becomes more extensive with increases in inlet sweep angle occurs in the inboard section of the inlets. The sweptforward inlets had, by comparison, much higher values of total pressure in the inboard section of the inlet for comparable forward-sweep angles. It seems obvious then that the boundary-layer-bypassing action, indicated previously to be the cause of the relative high pressure near the fuselage surface of the sweptforward inlet, must have been of very small magnitude in the case of the sweptback inlets. The oil-flow studies (figs. 8(c) and 8(d)) show that the bypassing action which did occur for the sweptback inlets at a Mach number of 1.4 was limited largely to the staggered or rearward lip and that the flow spillage at the fuselage surface decreased with increasing sweep angle. The reasons for the reduced spillage will be fairly evident from an examination of the schlieren photographs and the fuselage-nose pressure distributions (figs. 5(d) and (e) and fig. 4(b), respectively). The inlet terminal shock was very close to the most forward lip for all test conditions and was actually inside the forward lip of the 45° inlet at the highest mass-flow ratio; spillage required for particular values of inlet mass-flow ratio apparently occurred at the outboard portion of the inlet. Consequently, the distance available to bypass the boundary layer ahead of the inlet was very small. Furthermore, because the subsonic compression required to meet the inlet conditions was not complete for some distance downstream of the most rearward section of the inlet (figs. 4(a) and 4(b)), the pressure differential available for pumping or bypassing the boundary layer outside the inlet was low and decreased with increasing sweep angle.

A summary is presented in figure 9 of the maximum values of average total-pressure recovery obtained for the various combinations of inlet-lip sweep and stagger tested in the present investigation and in that of reference 2. The figure is a three-dimensional plot and presents results obtained at a mass-flow ratio of 0.6 at a Mach number of 1.4.

Flow Distortions at Inlet

The flow distortions for the several sweptforward and sweptback inlets are presented in figure 10 as a function of inlet mass-flow ratio for the test Mach number range. In general, the flow distortions decrease with reductions in mass-flow ratio at all test Mach numbers for both the sweptforward and sweptback inlets.

The sweptforward inlets had distortion values about equal to those of the unswept inlet. The maximum values of total distortion for the sweptforward inlets varied from 9.0 percent to 14 percent for maximum flow rates at Mach numbers of 1.0 and 1.4, respectively. As might be

expected, the lowest values of flow distortion and the highest pressure recoveries were obtained at the same values of mass-flow ratio. The sweptback inlets by comparison had much higher values of distortion as might also be expected from the pressure-recovery results. The maximum values of total distortion for these occurred for the 45° sweptback inlet and varied from 24 percent to 45 percent at Mach numbers of 1.0 and 1.4, respectively. (See fig. 10.)

Boundary-Layer Control

The unswept and sweptforward inlets had relatively high pressure recovery and low flow distortions largely because of natural bypassing of separated boundary layer. The sweptback inlets did not bypass significant quantities of boundary layer with resultant low recovery and high flow distortions. Inasmuch as the total-pressure recovery in the outboard sections of the sweptback inlets were generally higher than normal-shock recovery, several attempts were made to improve the boundary-layer-bypassing characteristics of these inlets. Four arbitrary modifications were made to the 45° sweptback inlet, which had the poorest performance of all inlets tested. The modifications included a semiswept inlet, a slotted semiswept inlet, a slotted 45° sweptback inlet, and a 45° sweptback inlet with a conventional boundary-layer diverter.

The first modification consisted of cutting off and, hence, unsweeping the inboard section of the inlet (fig. 11(a)) with the aim that the high outboard recoveries of the sweptback inlet would be retained while the bypassing action of the inboard sections would approach that of the unswept inlet. This modification (designated a semiswept inlet) did increase the bypassing at a Mach number of 1.4 (compare figs. 8(c) and (d) with fig. 12(a)) and produced small increases in pressure recovery; the maximum increase ($0.035p_{t,\infty}$) occurred at the low flow rates. (See fig. 13.) Large reductions in flow distortions, however, occurred throughout the mass-flow range.

The second modification was made to this semiswept inlet by cutting slots in both forward and rearward lips to allow some of the trapped boundary layer to escape. The slots, cut at the fuselage surface, were about 0.1 inch high and extended from the leading edge of each lip to the most rearward outboard section of the inlet. As shown in figures 12(a) and 12(b), the slot increased the bypassing with the result that the pressure recovery of the slotted semiswept inlet was 2 to 6 percent $p_{t,\infty}$ higher than that of the semiswept inlet at the high and low mass-flow ratios, respectively. (See fig. 13.) The maximum value of flow distortion, considerably lower than that of the semiswept inlet, was about equal to the maximum value obtained with the unswept inlet.

The third modification consisted of cutting a slot in each lip of the 45° sweptback inlet at the fuselage surface. As in the case of the slotted semiswept inlet, the slots were about 0.1 inch high and extended from the leading edge of each lip to the most rearward outboard section of the inlet; the slot length was necessarily longer for the fully swept inlet. The slots apparently bypassed large quantities of boundary layer (fig. 12(c)) with the result that the pressure recovery was appreciably higher than that of the 45° sweptback inlet without slots, the increases varying from 4 percent $p_{t,\infty}$ at the high flow rates to 7 percent $p_{t,\infty}$ at the low flow rates. (See fig. 13.) The pressure recovery obtained with the slotted 45° sweptback inlet was near the maximum obtained with the sweptforward inlets. Variations in mass-flow ratio had only small effects on the average total-pressure recovery. The maximum values of the total distortions decreased from 45 percent for the 45° sweptback inlet to about 18 percent for the slotted 45° sweptback inlet. (See fig. 13.)

The fourth and final modification consisted of installing a conventional boundary-layer diverter on the 45° sweptback inlet. (See fig. 11(b).) The leading edge of the splitter plate was cut off flush with the inlet lips and was 0.1 inch high. As shown in figure 13, the pressure recovery of this configuration and the slotted 45° sweptback inlet were about the same ($0.94p_{t,\infty}$) at the high flow rates and the pressure recovery of the slotted 45° sweptback inlet was higher at mass-flow ratios of 0.7 and below. The flow distortions of the inlet with a boundary-layer diverter are slightly higher than those of the slotted 45° sweptback inlet throughout the mass-flow-ratio range.

Inlet Performance

The results of the present investigation indicate that, from the standpoint of both inlet pressure recovery and flow distortion, the slotted semiswept inlet and the sweptforward inlets are superior to the other configurations tested. The optimum mass-flow ratio (highest pressure recovery and lowest flow distortion), however, appears to be somewhat lower for the slotted semiswept inlet than for the sweptforward inlets. In order to compare the overall performance of one inlet with another, the external drag as well as both pressure recovery and flow distortions must be considered. The external drag of an inlet operating at low flow rates would be greater than that of a similar inlet operating at a higher flow rate largely because of an increase in spillage drag. The overall optimum mass-flow ratio, therefore, would probably be higher than the mass-flow ratio indicated by consideration of the pressure recovery and flow distortions alone.

SUMMARY OF RESULTS

An investigation has been made in the Langley transonic blowdown tunnel to study the effects of inlet-lip sweep angle on the internal flow characteristics of a semielliptical scoop-type inlet with 30° of lip stagger. The inlet sweep angle was varied from 45° sweepforward to 45° sweepback in increments of 15°. Tests were made at Mach numbers of 1.0, 1.2, and 1.4 through a mass-flow-ratio range of 0.4 to 0.9 at an angle of attack of 0°. The more important results are summarized as follows:

1. The average total-pressure recovery and flow distortions of the sweptforward inlets were superior to those of the sweptback inlets at all test conditions. The maximum pressure recovery obtained was near the maximum obtainable through a normal shock.

2. At a Mach number of 1.4, increases in inlet forward sweep angle produced improvements in both pressure recovery and flow uniformity at the high mass-flow ratios when compared with an unswept inlet whereas increases in inlet sweepback always produced adverse effects on the pressure recovery and flow uniformity.

3. The improved performance of the sweptforward inlets was attributed largely to a more complete bypassing of the fuselage boundary layer.

4. A simple slot cut in the lips of the 45° sweptback inlet improved the pressure recovery and flow uniformity of this inlet equally as well as a conventional boundary-layer diverter of the same height. The pressure recovery obtained with the slotted 45° sweptback inlet was near the maximum obtained with the sweptforward inlets.

Langley Aeronautical Laboratory,
National Advisory Committee for Aeronautics,
Langley Field, Va., April 22, 1957.

REFERENCES

1. Bingham, Gene J.: Investigation at Transonic Speeds of the Aerodynamic Characteristics of an Unswept Semielliptical Air Inlet in the Root of a 45° Sweptback Wing. NACA RM L55F22a, 1955.

2. Bingham, Gene J., and Trescot, Charles D., Jr.: Investigation at Transonic Speeds of the Effects of Inlet Lip Stagger on the Internal-Flow Characteristics of an Unswept Semielliptical Air Inlet. NACA RM L56C22, 1956.

3. Nussdorfer, T. J.: Some Observations of Shock-Induced Turbulent Separation on Supersonic Diffusers. NACA RM E51L26, 1954.

TABLE I - DESIGN COORDINATES FOR NOSE AND INLET SECTIONS

(All dimensions are in inches)

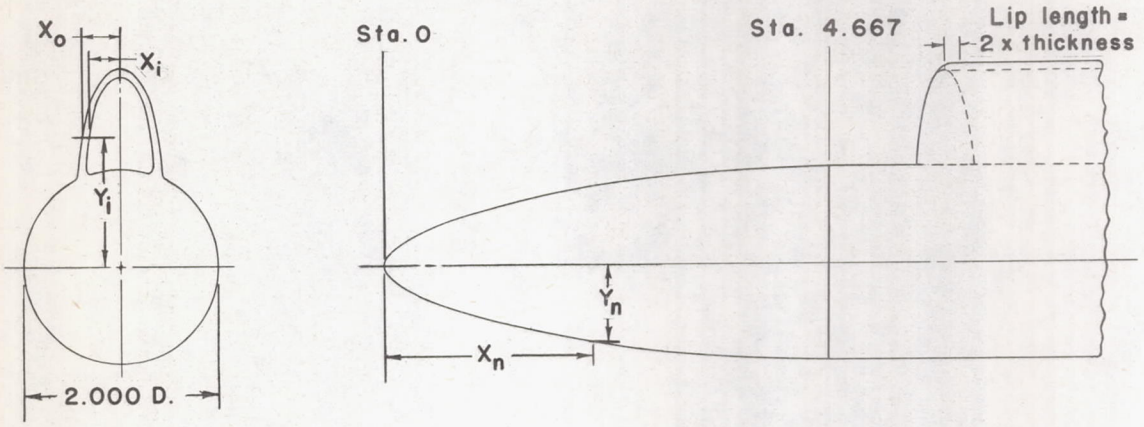

Coordinates for inlet section		
Y_i	X_i	X_o
0.900		0.429
.960	0.315	.429
.980	.343	.429
1.000	.354	.429
1.050	.352	.429
1.100	.350	.425
1.200	.344	.419
1.300	.332	.407
1.400	.318	.393
1.500	.301	.376
1.600	.277	.352
1.700	.246	.325
1.800	.205	.285
1.850	.180	.267
1.900	.142	.240
1.925	.129	.223
1.950	.105	.205
1.960	.090	
1.970	.072	
1.980	.065	
1.990	.042	
2.000	.000	.155
2.025		.130
2.050		.080
2.075		.000

Coordinates for nose contour	
X_n	Y_n
0.000	0.000
.019	.066
.037	.093
.047	.104
.070	.127
.093	.147
.140	.183
.187	.215
.233	.244
.327	.295
.420	.340
.560	.401
.700	.453
.933	.527
1.167	.592
1.400	.649
1.866	.748
2.333	.827
2.706	.880
2.986	.912
3.173	.931
3.546	.962
3.919	.983
4.293	.997
4.667	1.000

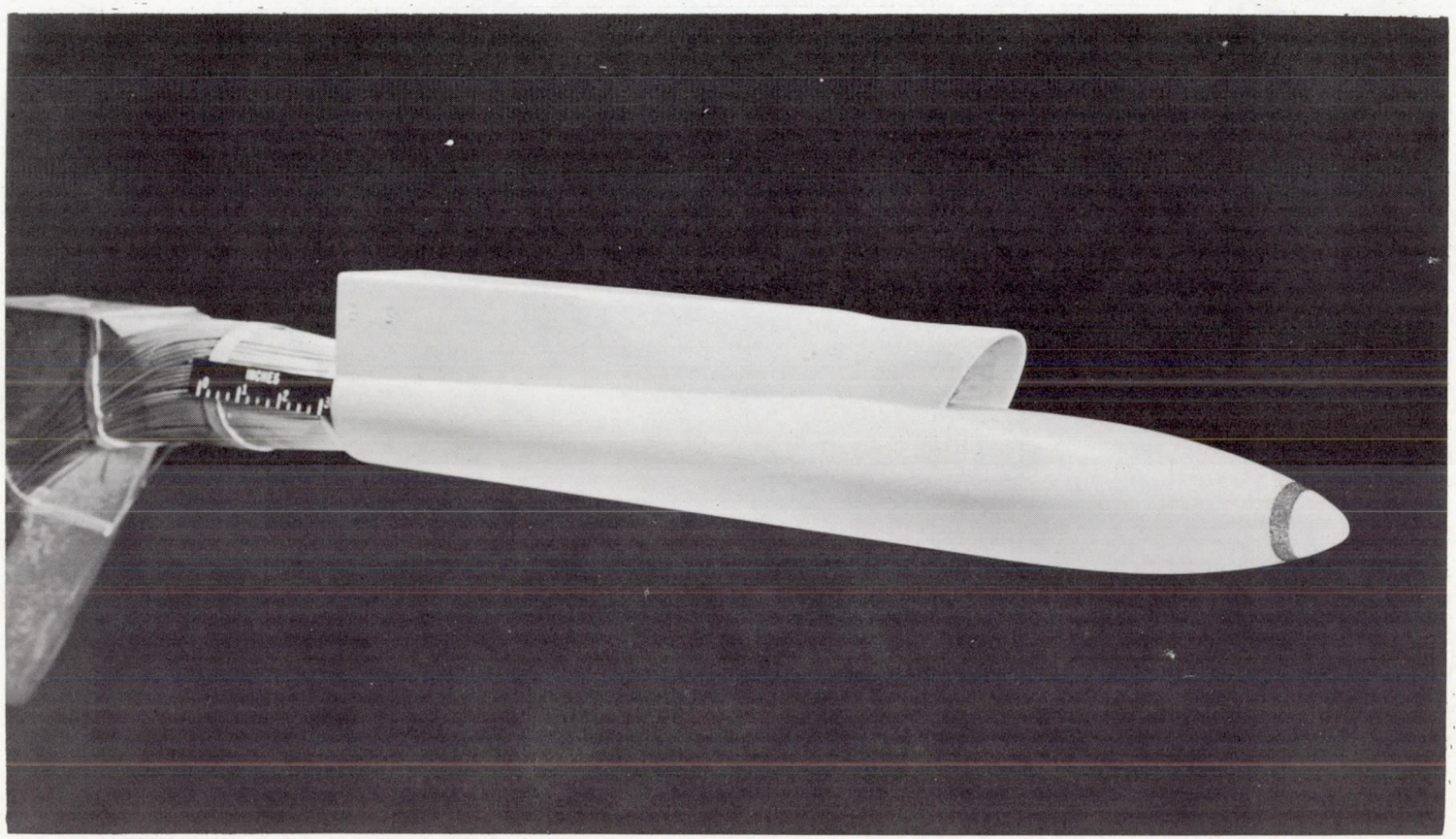

L-89158

Figure 1.- Three-quarter front view of inlet model with 30° forward sweep.

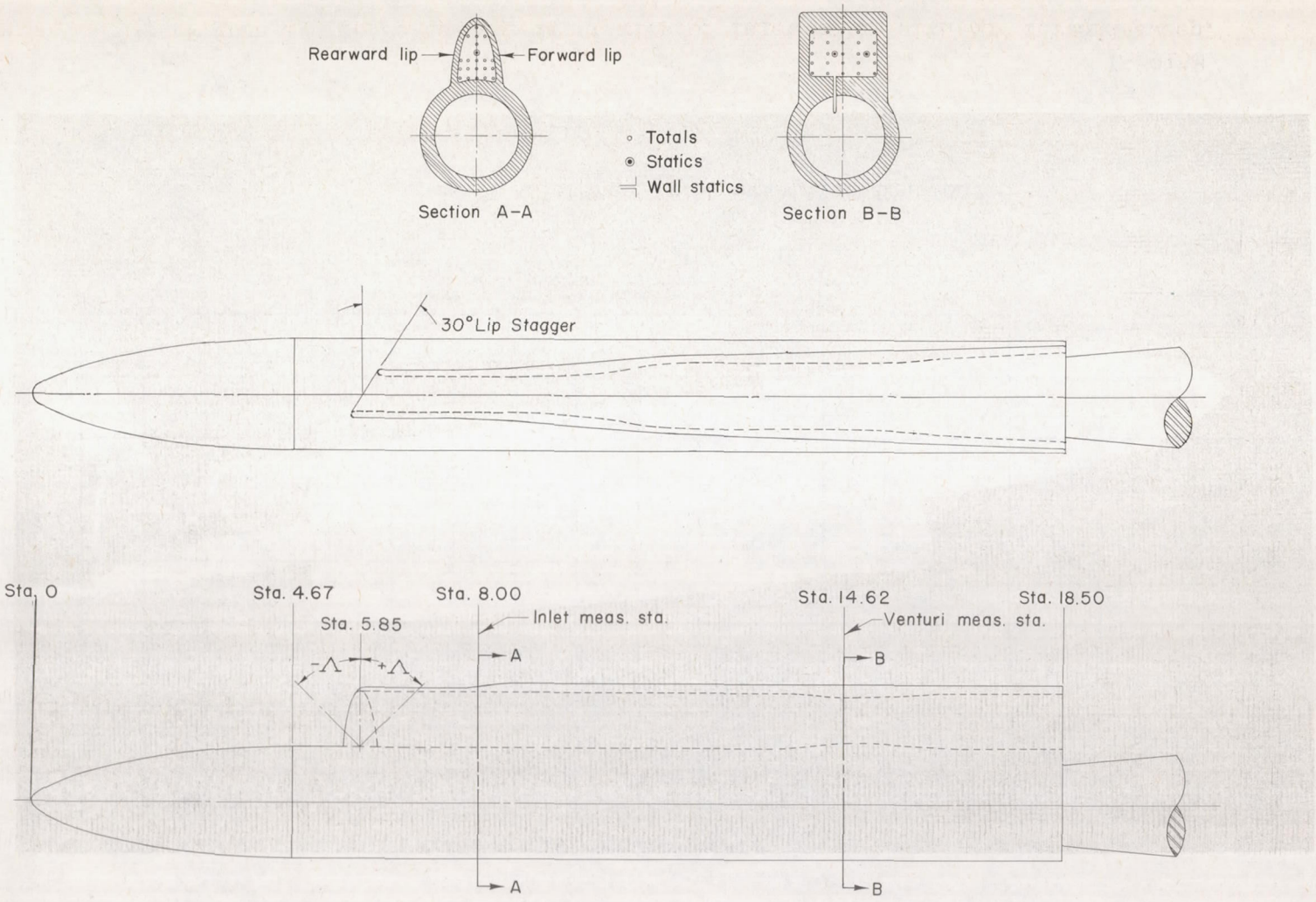

Figure 2.- View of model showing internal ducting and total-pressure measuring stations. All dimensions are in inches.

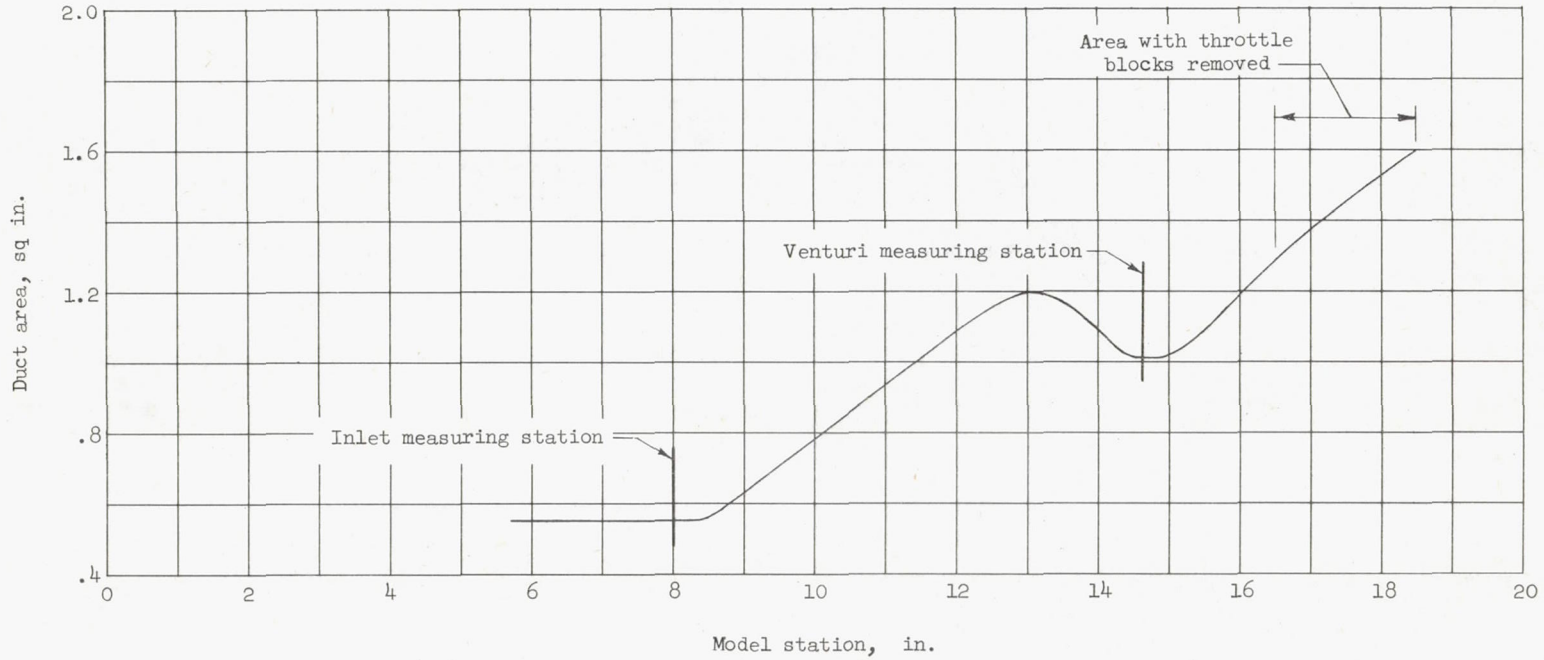

Figure 3.- Internal duct area distribution.

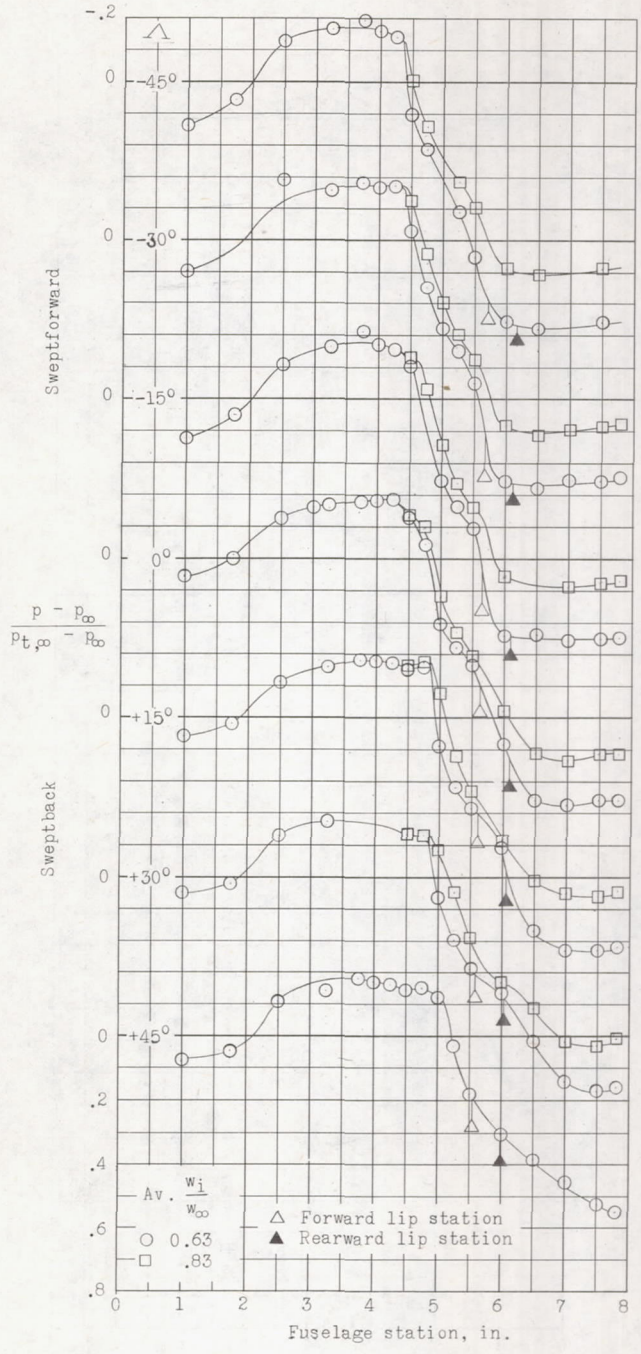

(a) $M_\infty = 1.0$.

Figure 4.- Surface static-pressure distributions along the vertical center line.

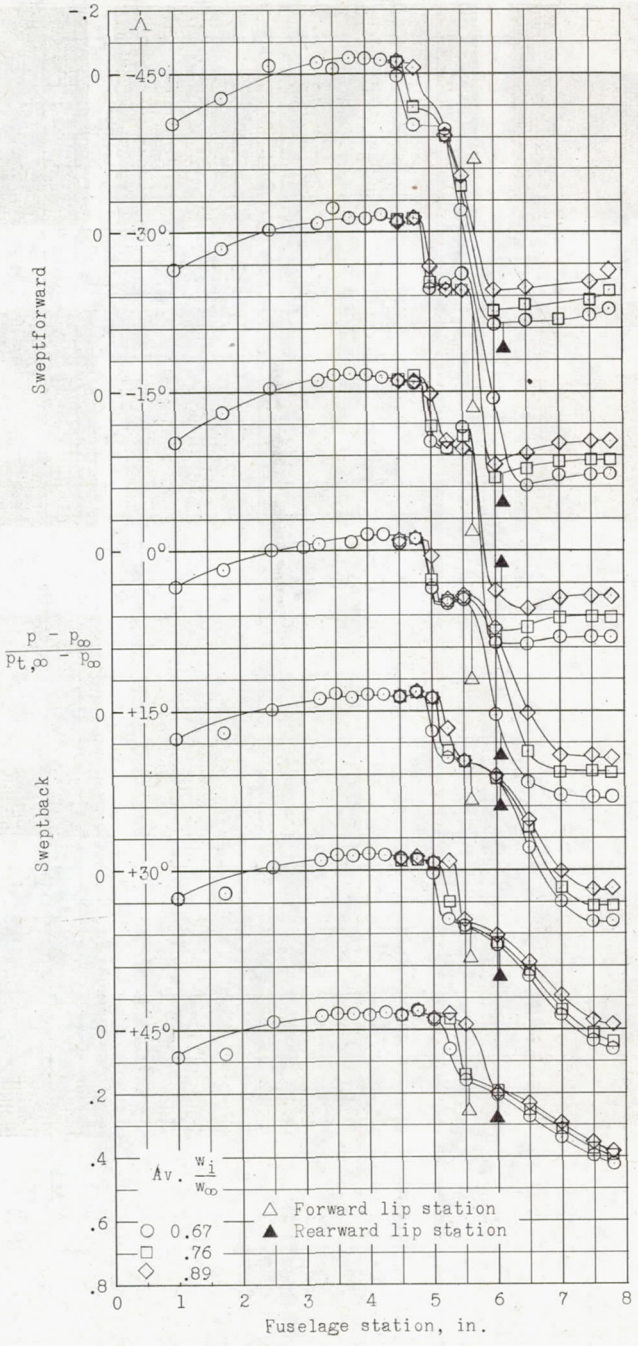

(b) $M_\infty = 1.4$.

Figure 4.- Concluded.

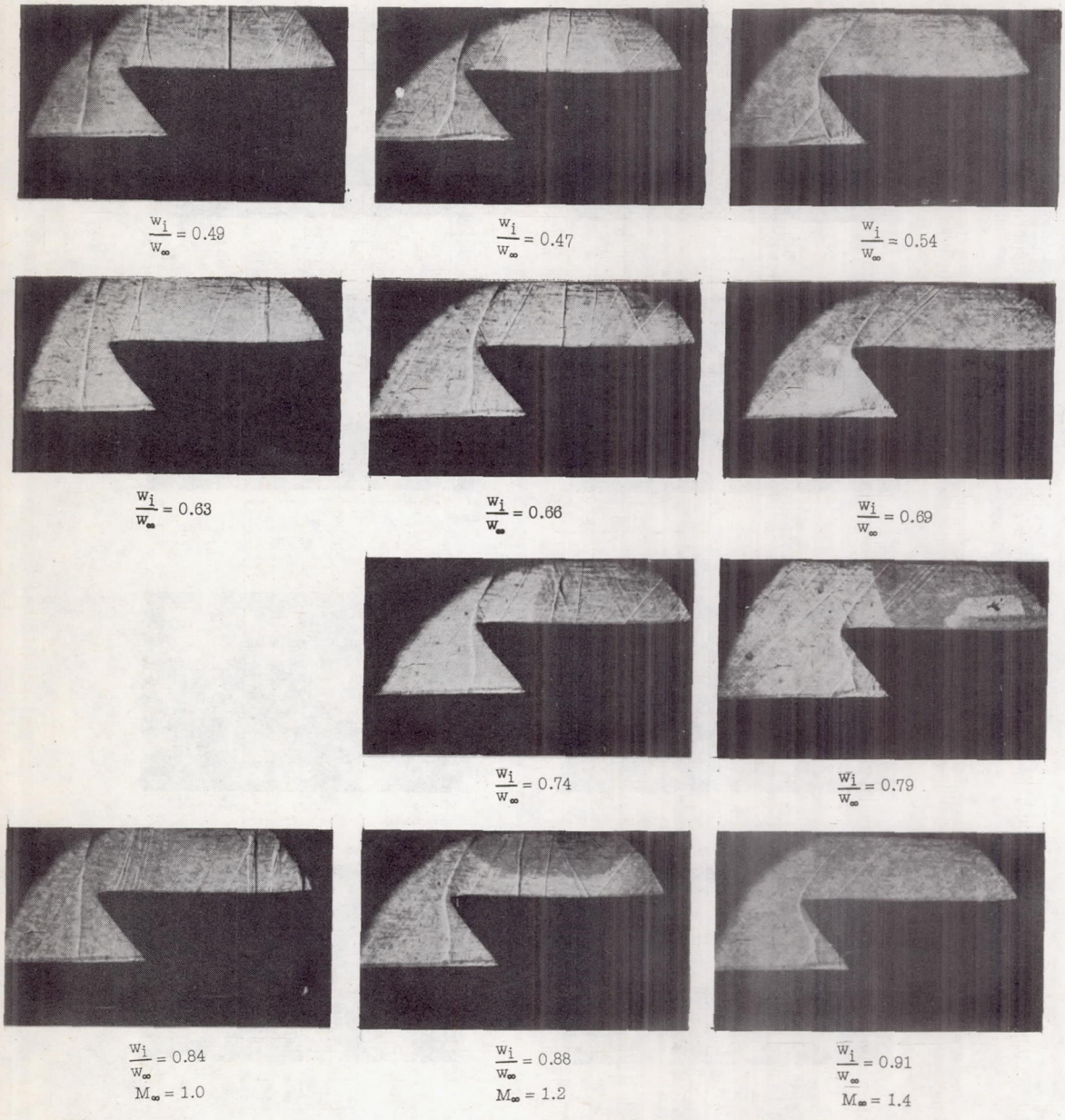

(a) 45° sweptforward inlet. L-57-1573

Figure 5.- Schlieren photographs of the flow about the several inlet configurations.

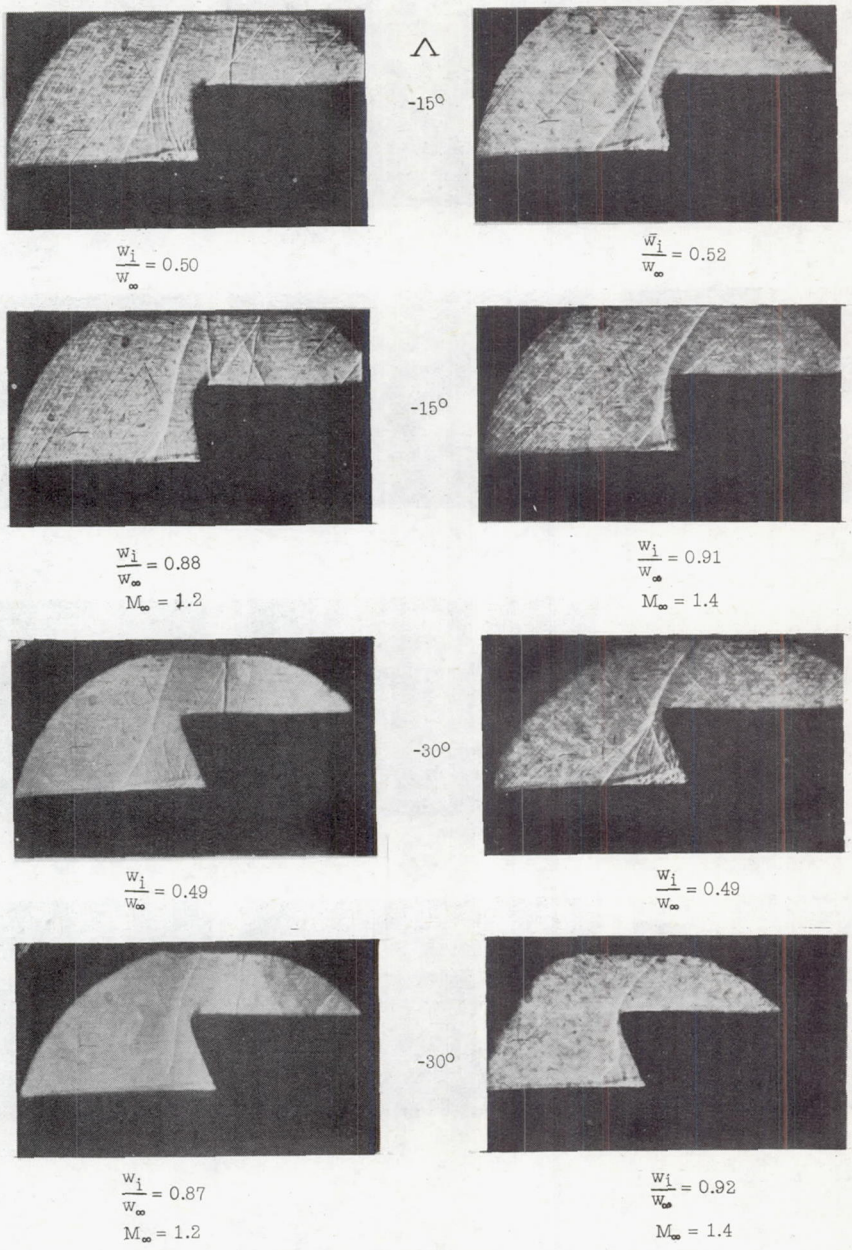

(b) 15° and 30° sweptforward inlets. L-57-1574

Figure 5.- Continued.

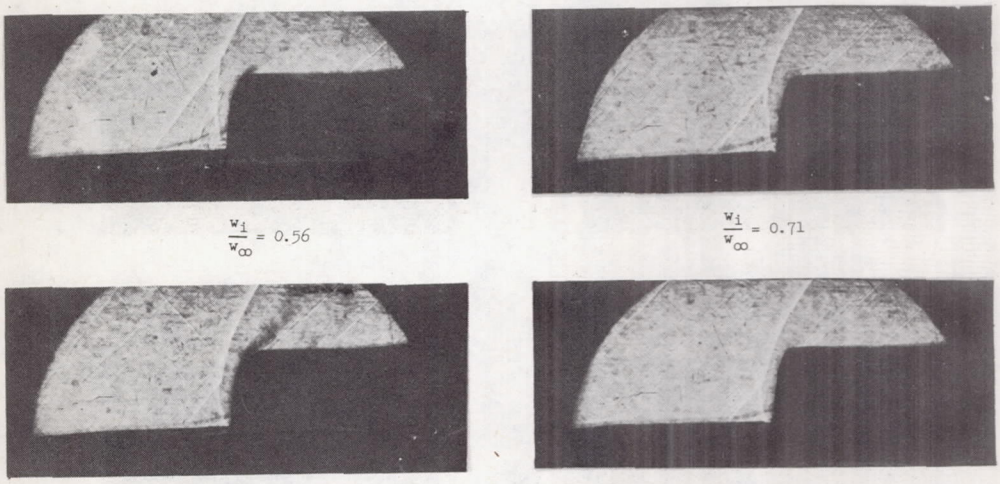

$\frac{w_i}{w_\infty} = 0.56$ $\frac{w_i}{w_\infty} = 0.71$

$\frac{w_i}{w_\infty} = 0.78$ $\frac{w_i}{w_\infty} = 0.90$

$M_\infty = 1.4$

(c) Unswept inlet. L-57-1575

Figure 5.- Continued.

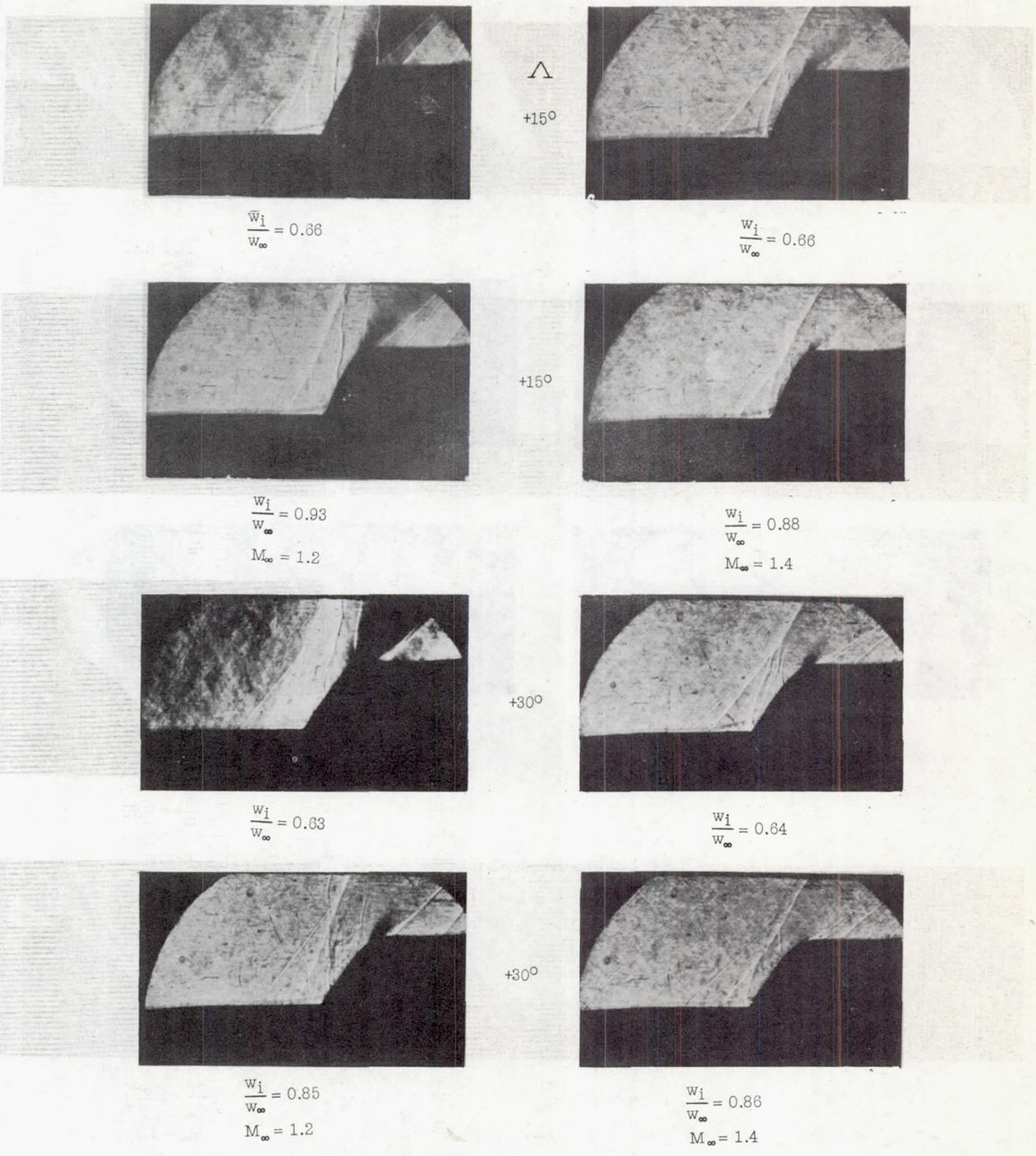

(d) 15° and 30° sweptback inlets. L-57-1576

Figure 5.- Continued.

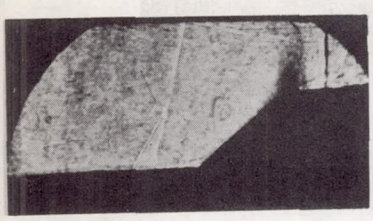

$\frac{w_i}{w_\infty} = 0.46$

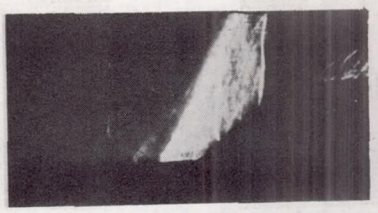

$\frac{w_i}{w_\infty} = 0.46$

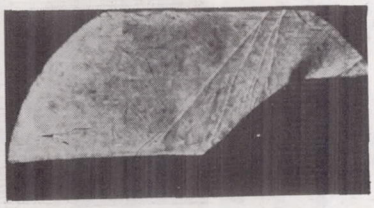

$\frac{w_i}{w_\infty} = 0.43$

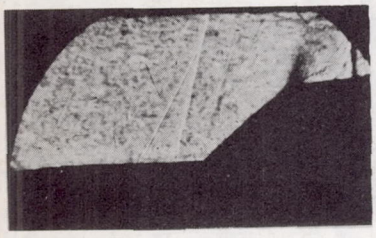

$\frac{w_i}{w_\infty} = 0.63$

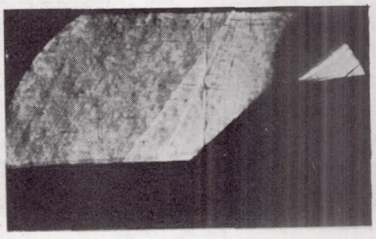

$\frac{w_i}{w_\infty} = 0.64$

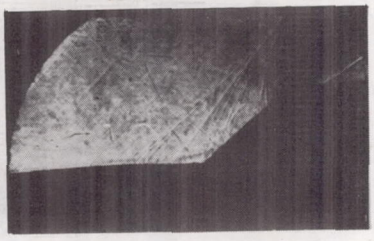

$\frac{w_i}{w_\infty} = 0.61$

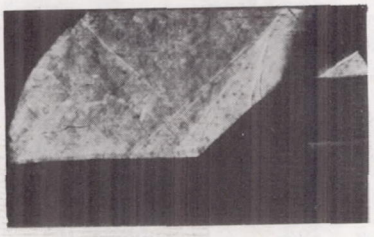

$\frac{w_i}{w_\infty} = 0.70$

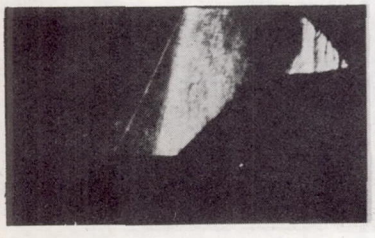

$\frac{w_i}{w_\infty} \approx 0.85$

$M_\infty = 1.0$

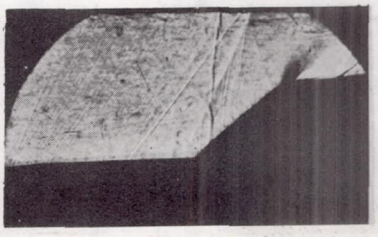

$\frac{w_i}{w_\infty} = 0.86$

$M_\infty = 1.2$

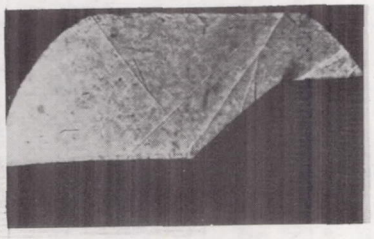

$\frac{w_i}{w_\infty} = 0.86$

$M_\infty = 1.4$

(e) 45° sweptback inlet. L-57-1577

Figure 5.- Concluded.

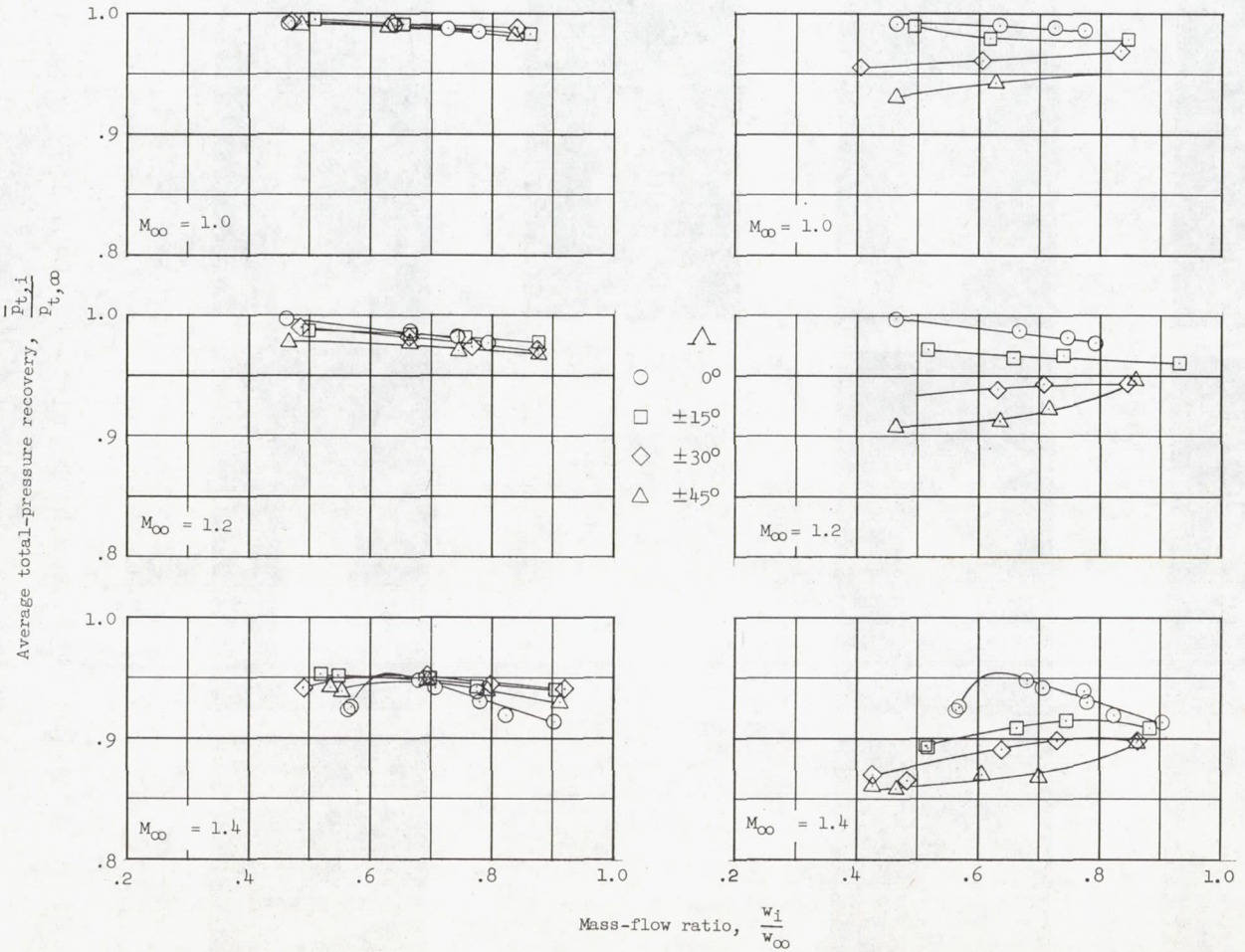

(a) Sweptforward inlet.

(b) Sweptback inlet.

Figure 6.- Effect of variations in mass-flow ratio, Mach number, and inlet-lip sweep on total-pressure recovery at inlet measuring station.

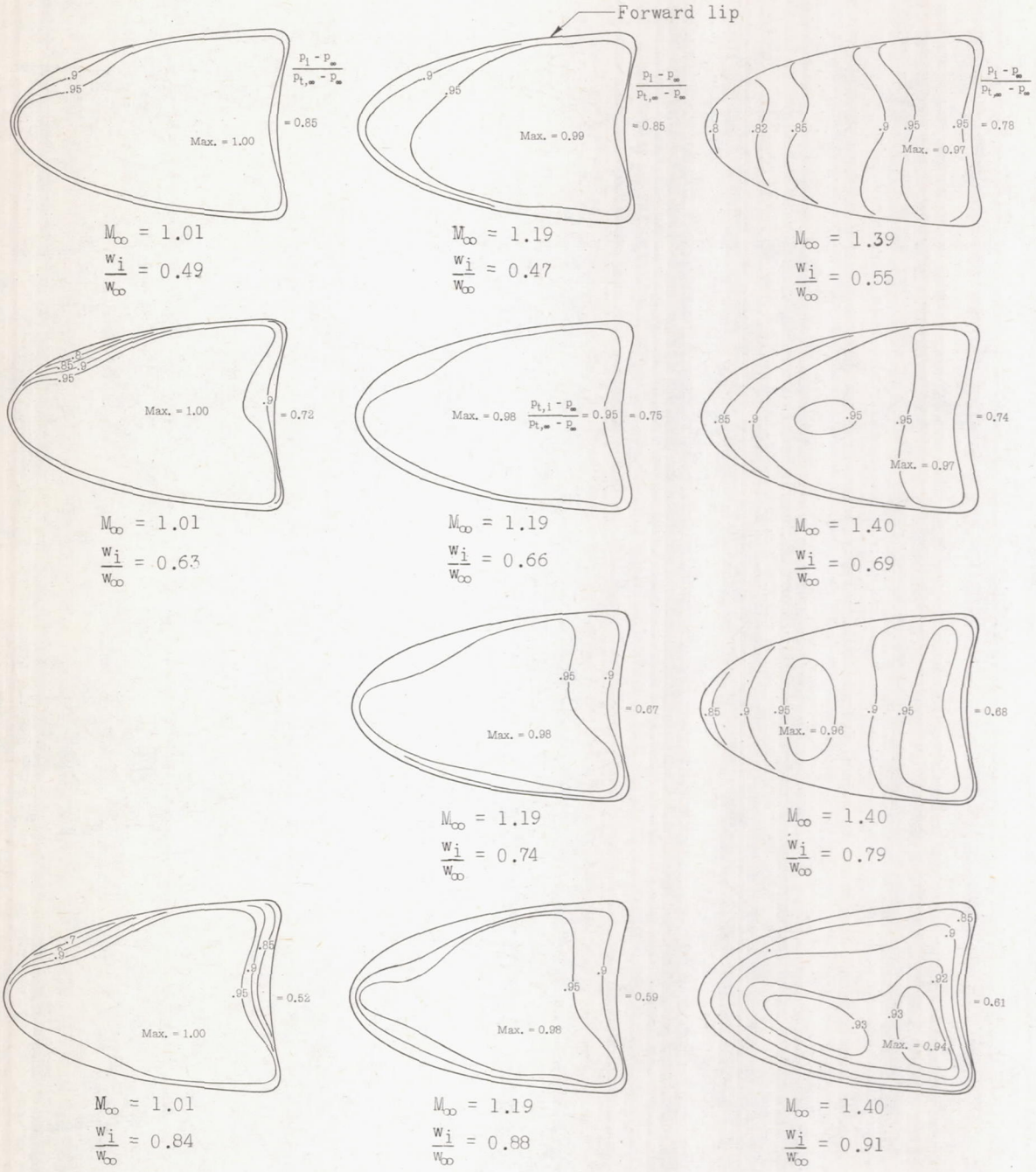

(a) 45° sweptforward inlet.

Figure 7.- Contours of impact-pressure ratio at inlet measuring station for various angles of inlet-lip sweep.

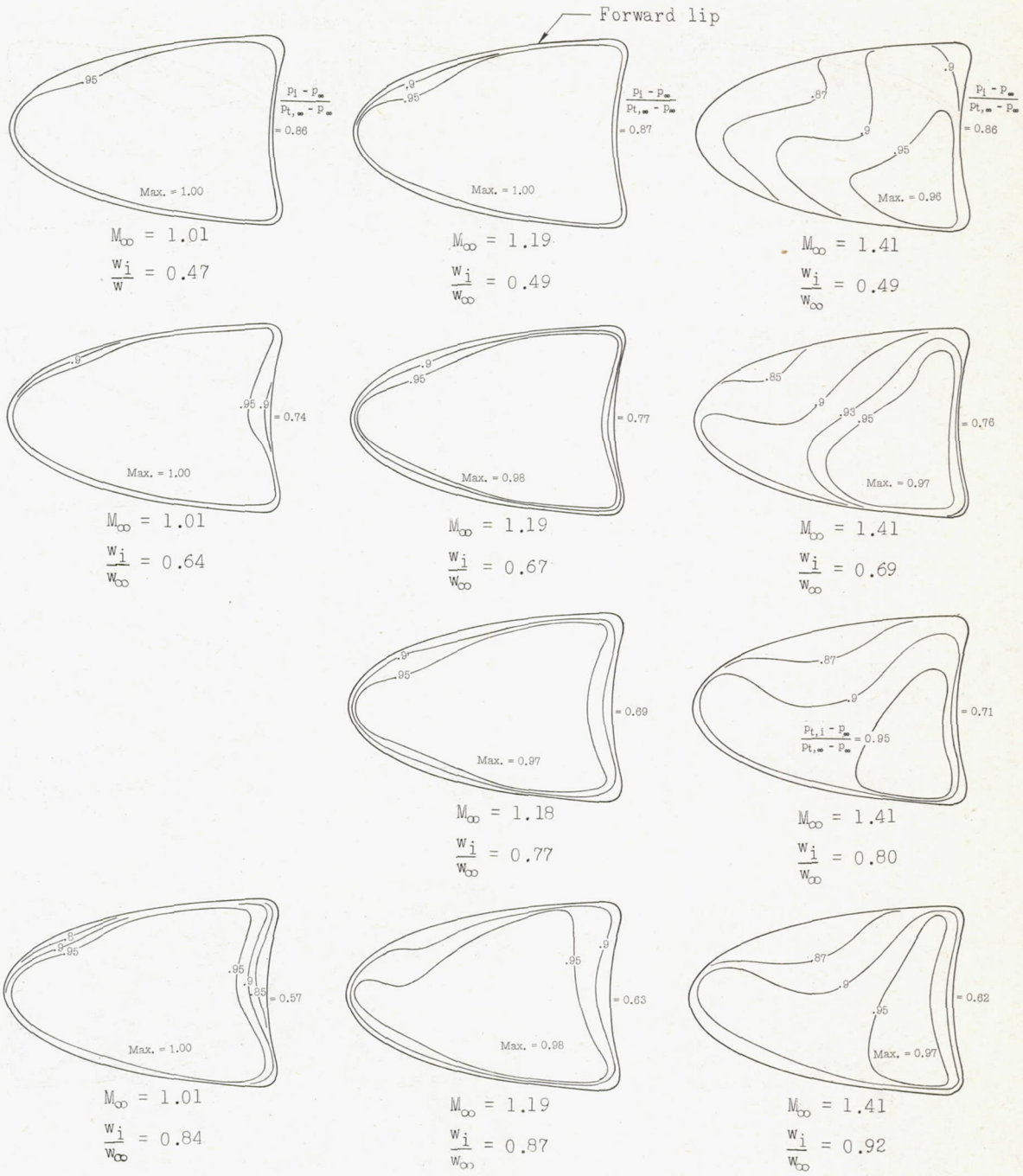

(b) 30° sweptforward inlet.

Figure 7.- Continued.

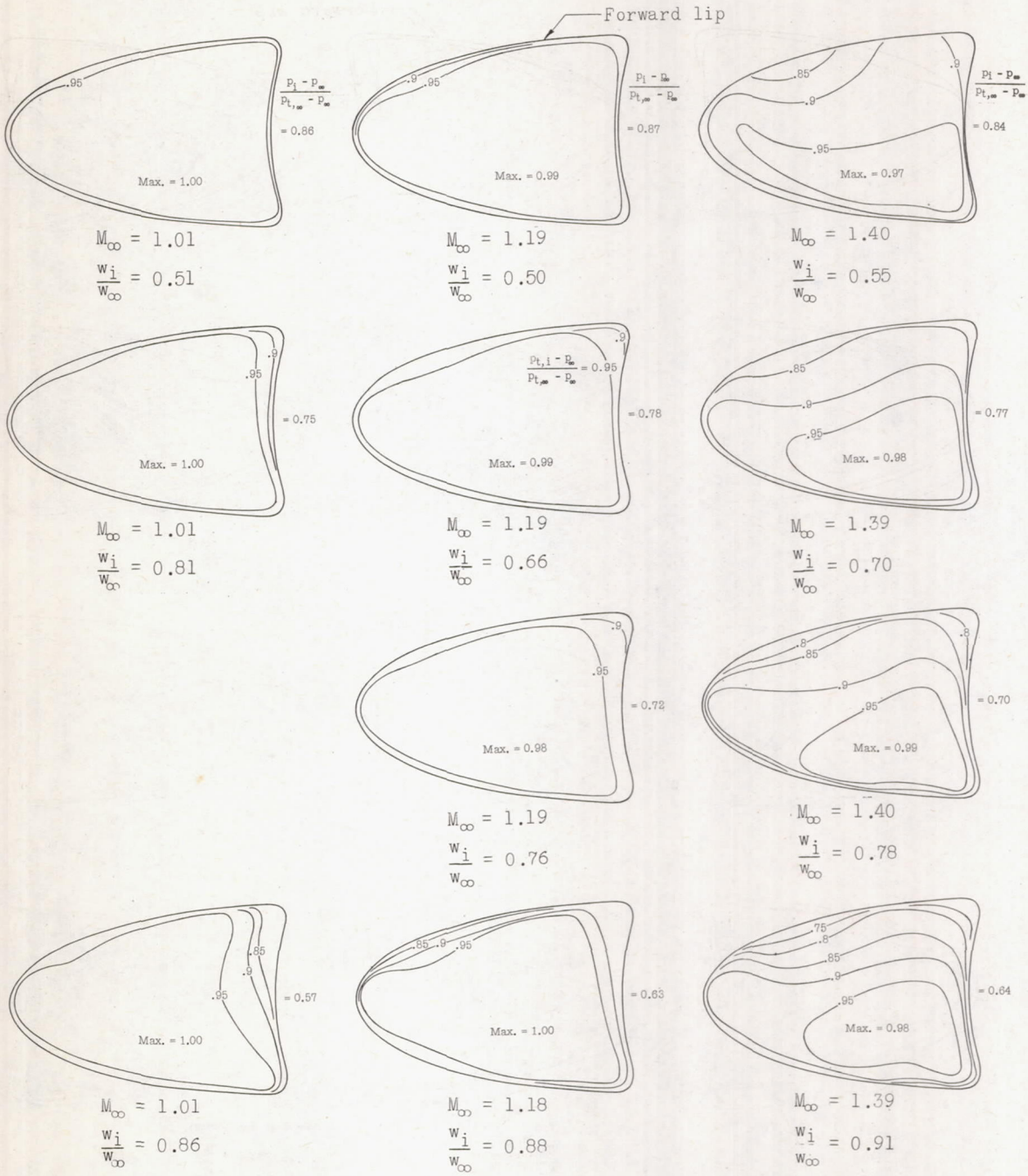

(c) 15° sweptforward inlet.

Figure 7.- Continued.

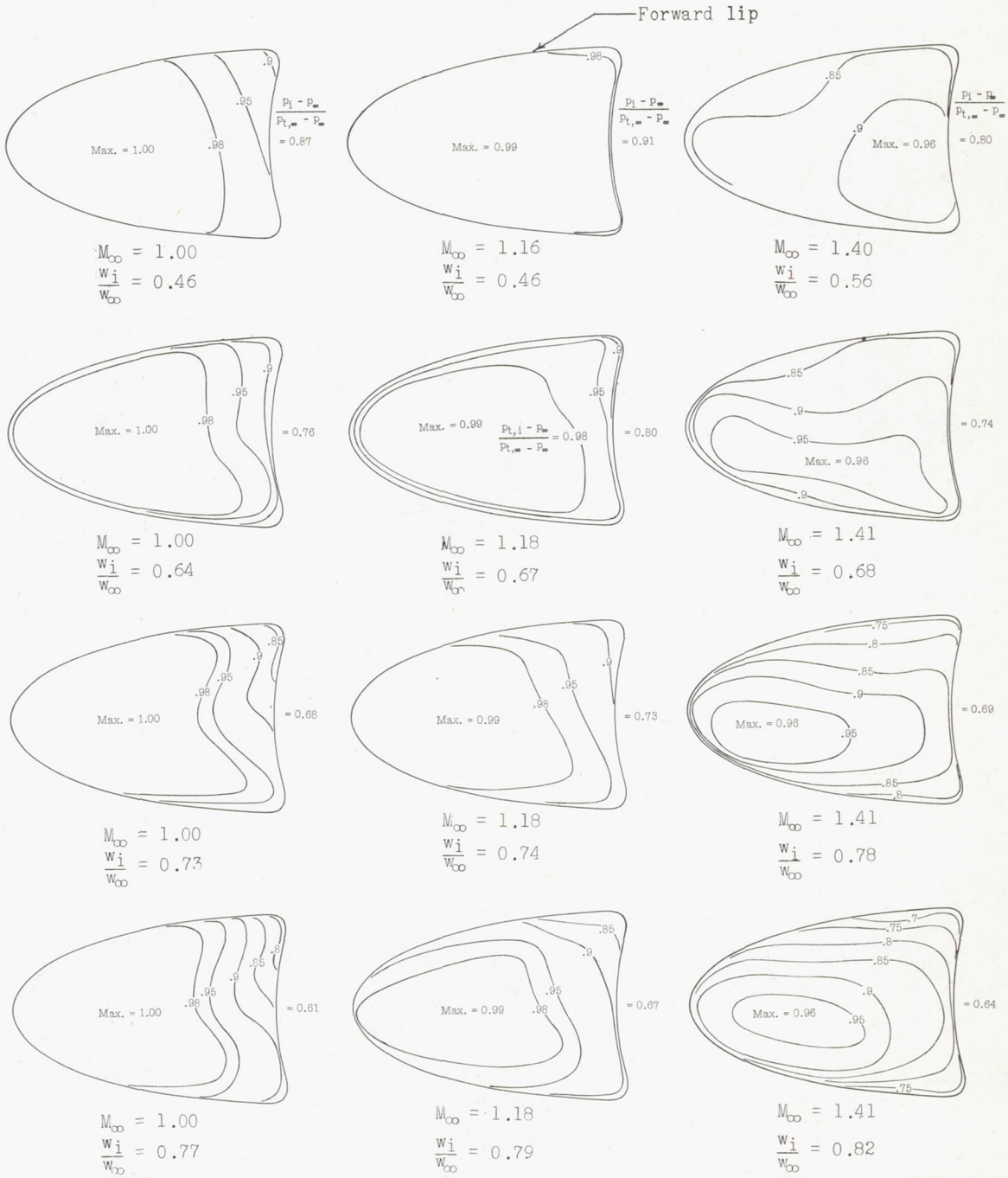

(d) Unswept inlet.

Figure 7.- Continued.

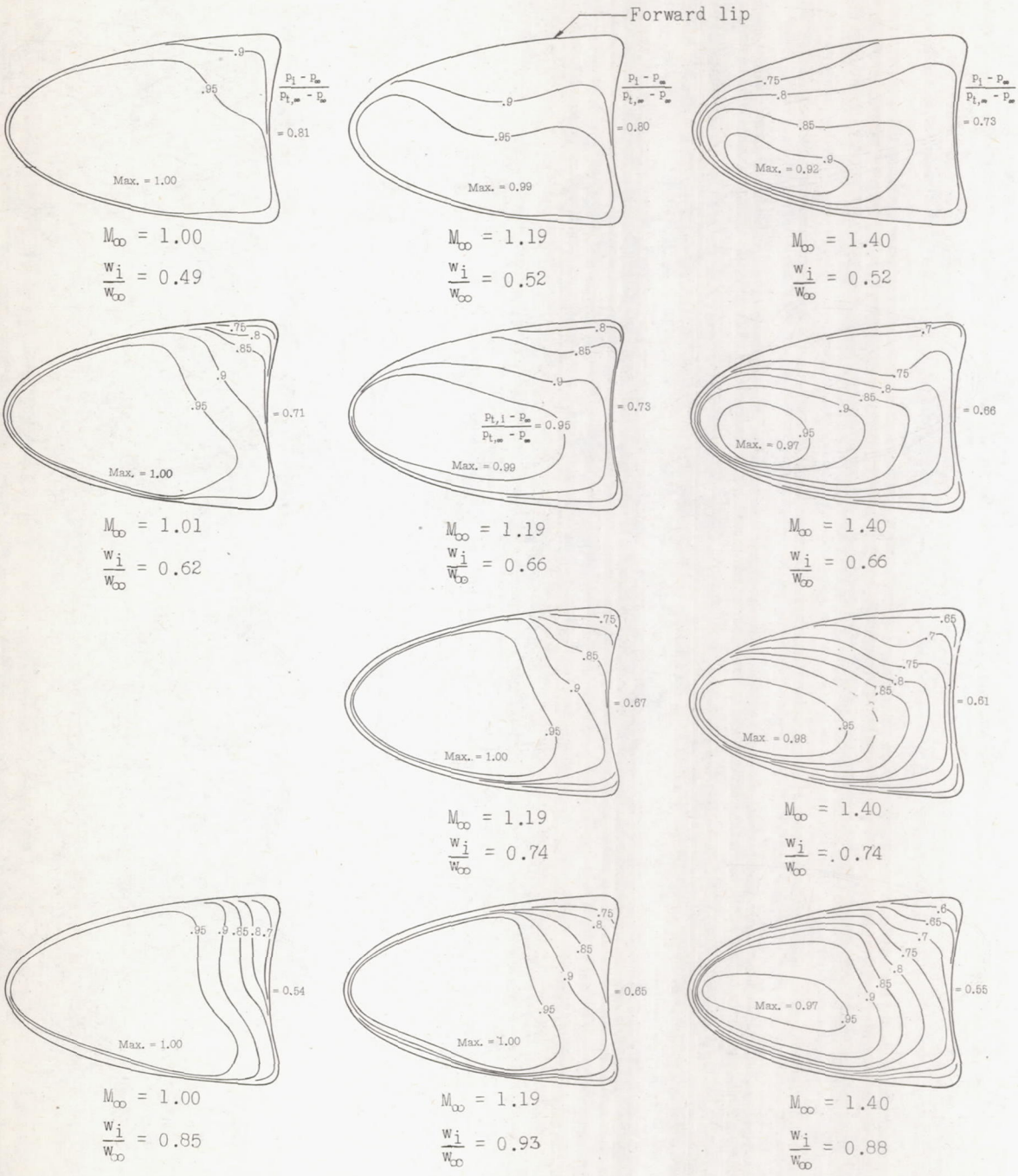

(e) 15° sweptback inlet.

Figure 7.- Continued.

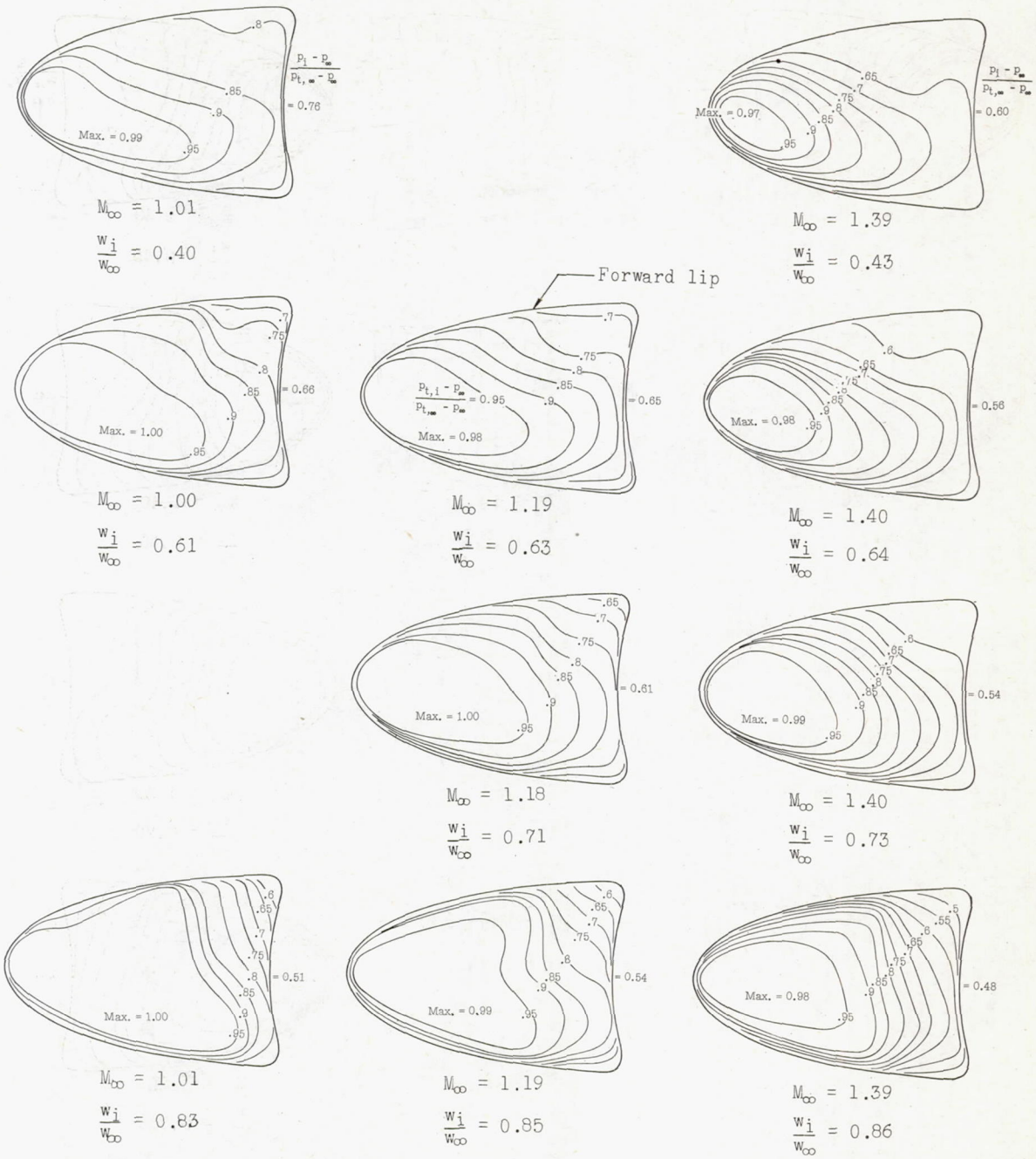

$M_\infty = 1.01$ $\frac{w_i}{w_\infty} = 0.40$

$M_\infty = 1.39$ $\frac{w_i}{w_\infty} = 0.43$

$M_\infty = 1.00$ $\frac{w_i}{w_\infty} = 0.61$

$M_\infty = 1.19$ $\frac{w_i}{w_\infty} = 0.63$

$M_\infty = 1.40$ $\frac{w_i}{w_\infty} = 0.64$

$M_\infty = 1.18$ $\frac{w_i}{w_\infty} = 0.71$

$M_\infty = 1.40$ $\frac{w_i}{w_\infty} = 0.73$

$M_\infty = 1.01$ $\frac{w_i}{w_\infty} = 0.83$

$M_\infty = 1.19$ $\frac{w_i}{w_\infty} = 0.85$

$M_\infty = 1.39$ $\frac{w_i}{w_\infty} = 0.86$

(f) 30° sweptback inlet.

Figure 7.- Continued.

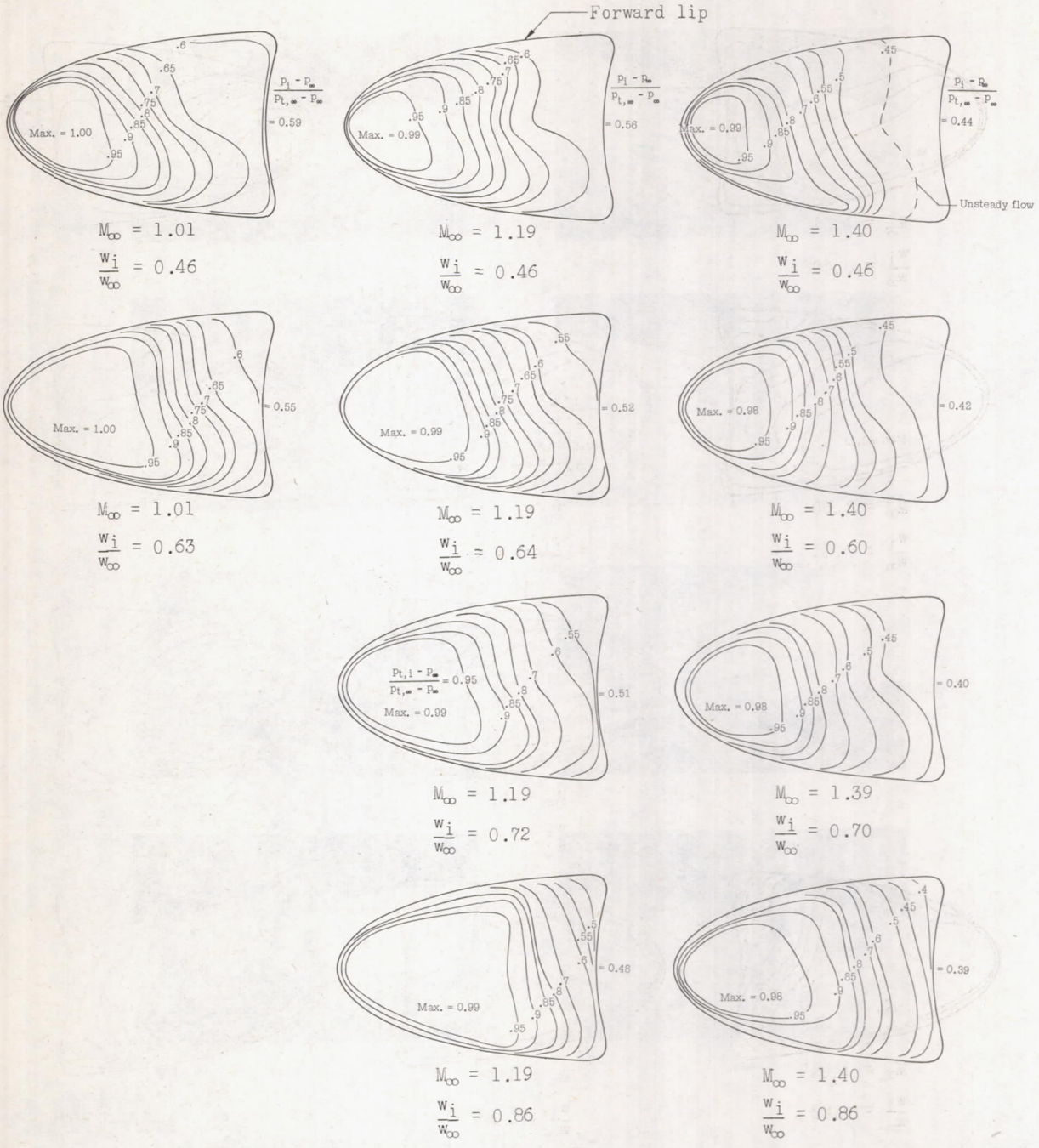

(g) 45° sweptback inlet.

Figure 7.- Concluded.

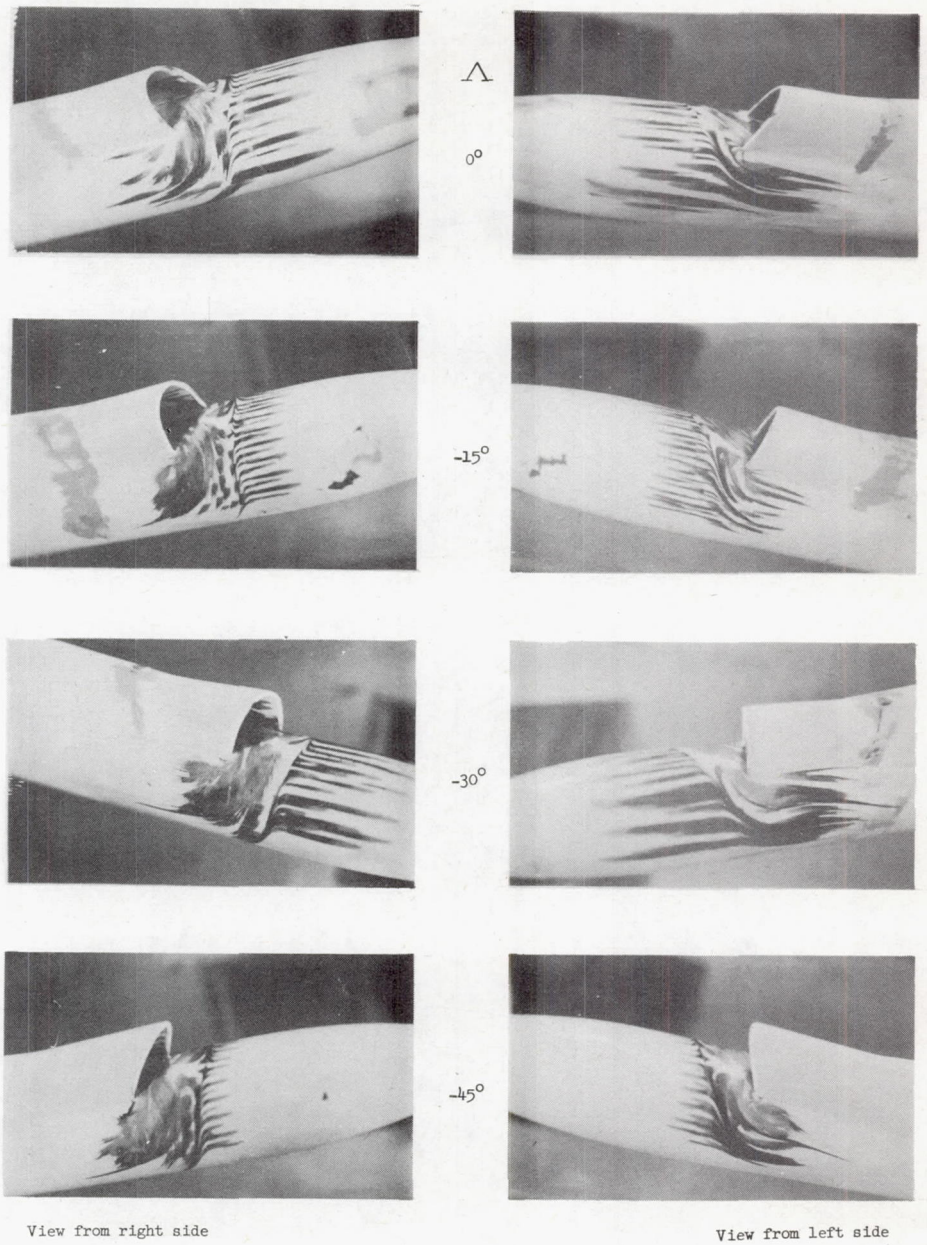

L-57-1578

(a) $\Lambda = 0^\circ$, -15°, -30°, and -45°; $w_1/w_\infty \approx 0.70$.

Figure 8.- The effect of inlet sweep angle and mass-flow ratio on the flow within the boundary layer as indicated by the oil-flow traces at $M_\infty = 1.4$.

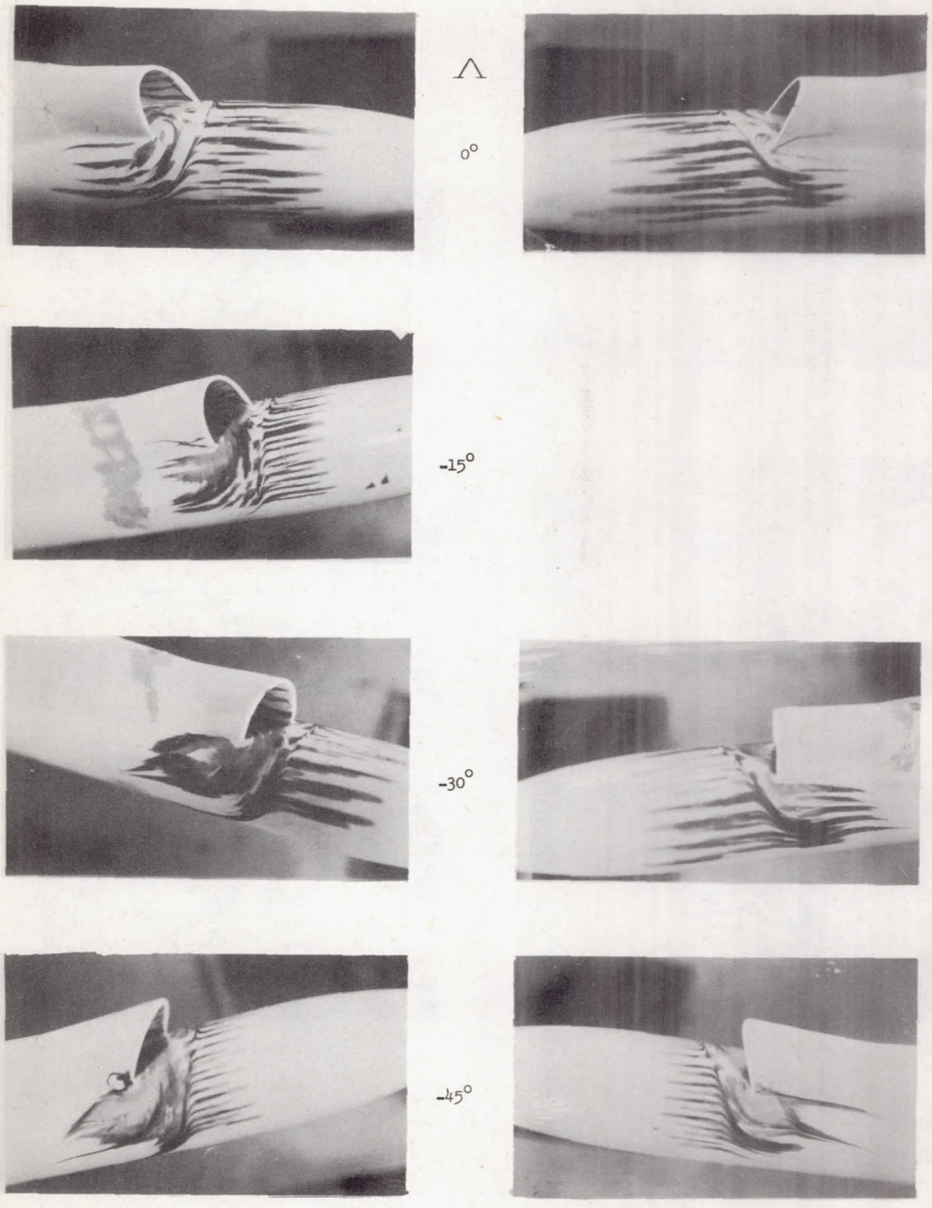

L-57-1579

(b) $\Lambda = 0^\circ, -15^\circ, -30^\circ$, and -45°; $w_i/w_\infty \approx 0.91$.

Figure 8.- Continued.

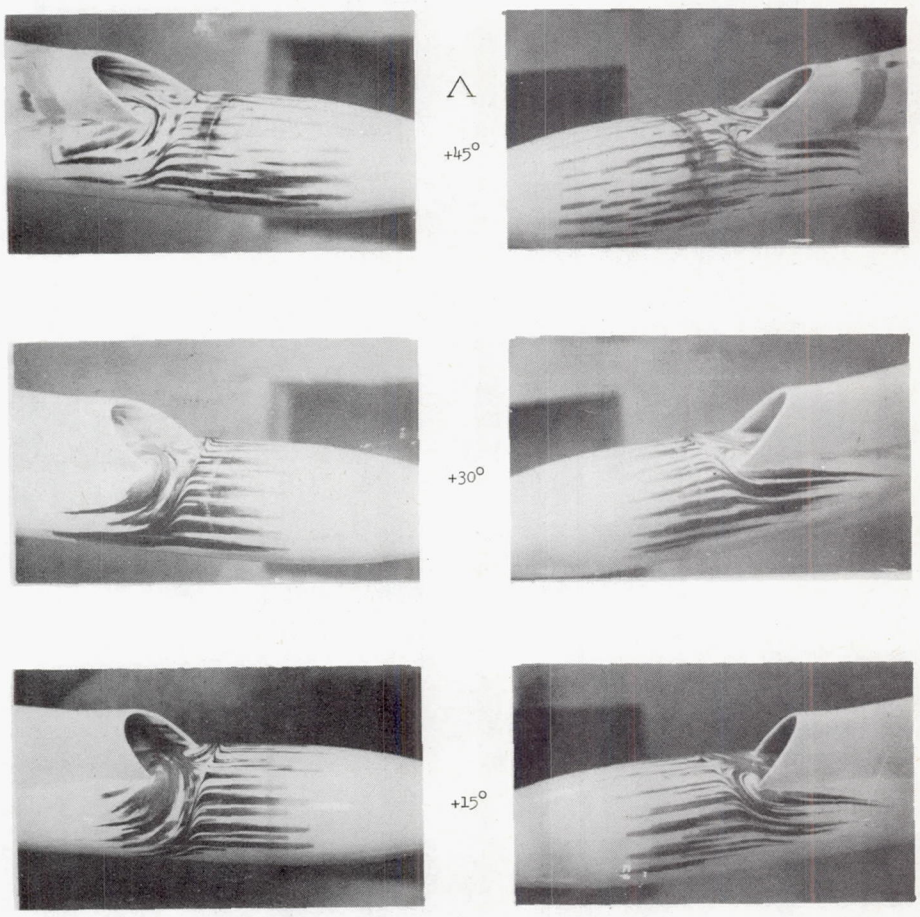

L-57-1580

(c) $\Lambda = 45^\circ$, 30°, and 15°; $w_i/w_\infty \approx 0.63$.

Figure 8.- Continued.

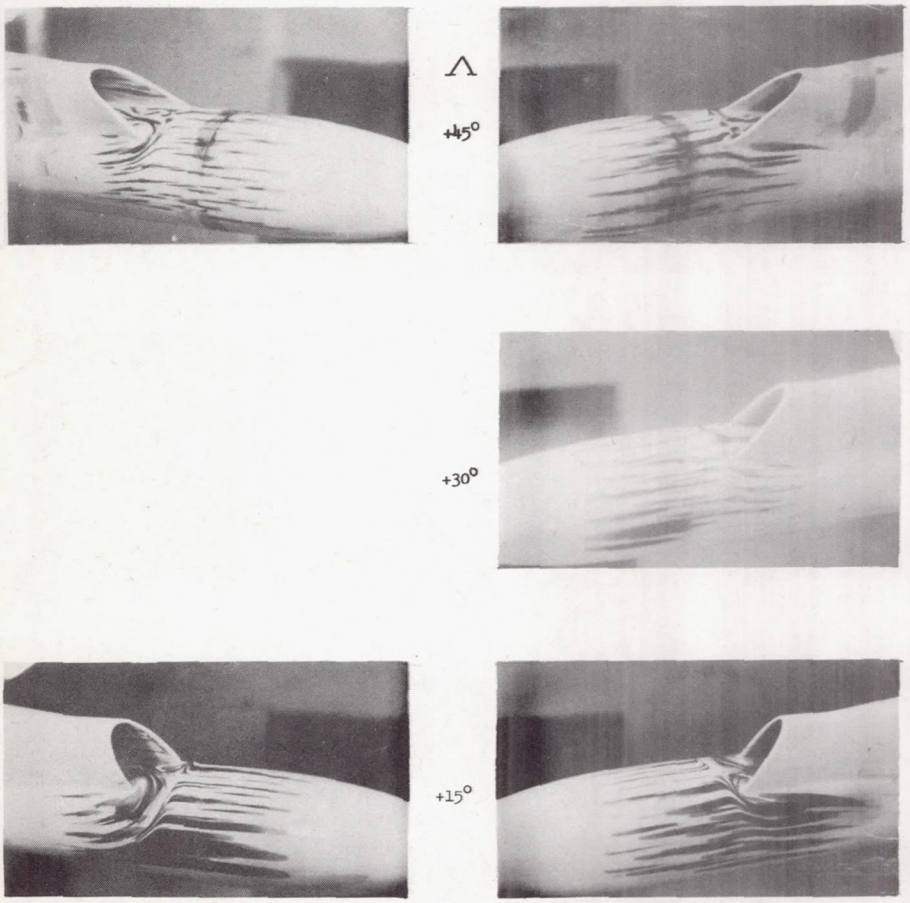

(d) $\Lambda = 45^\circ$, 30°, and 15°; $w_i/w_\infty \approx 0.87$. L-57-1581

Figure 8.- Concluded.

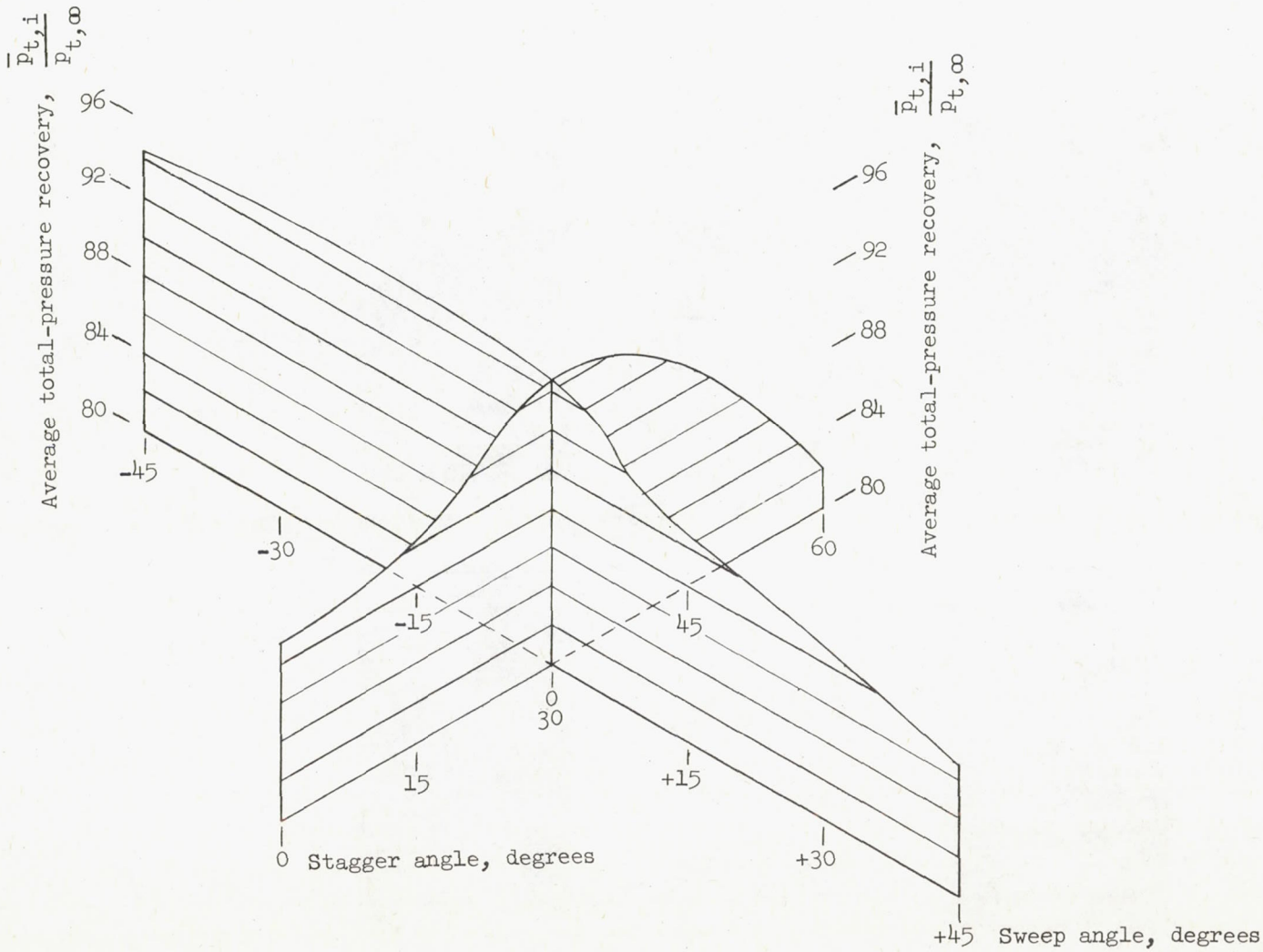

Figure 9.- Three-dimensional plot of variation of average total-pressure recovery with inlet-lip sweep and stagger $w_i/w_\infty = 0.6$; $M_\infty = 1.4$.

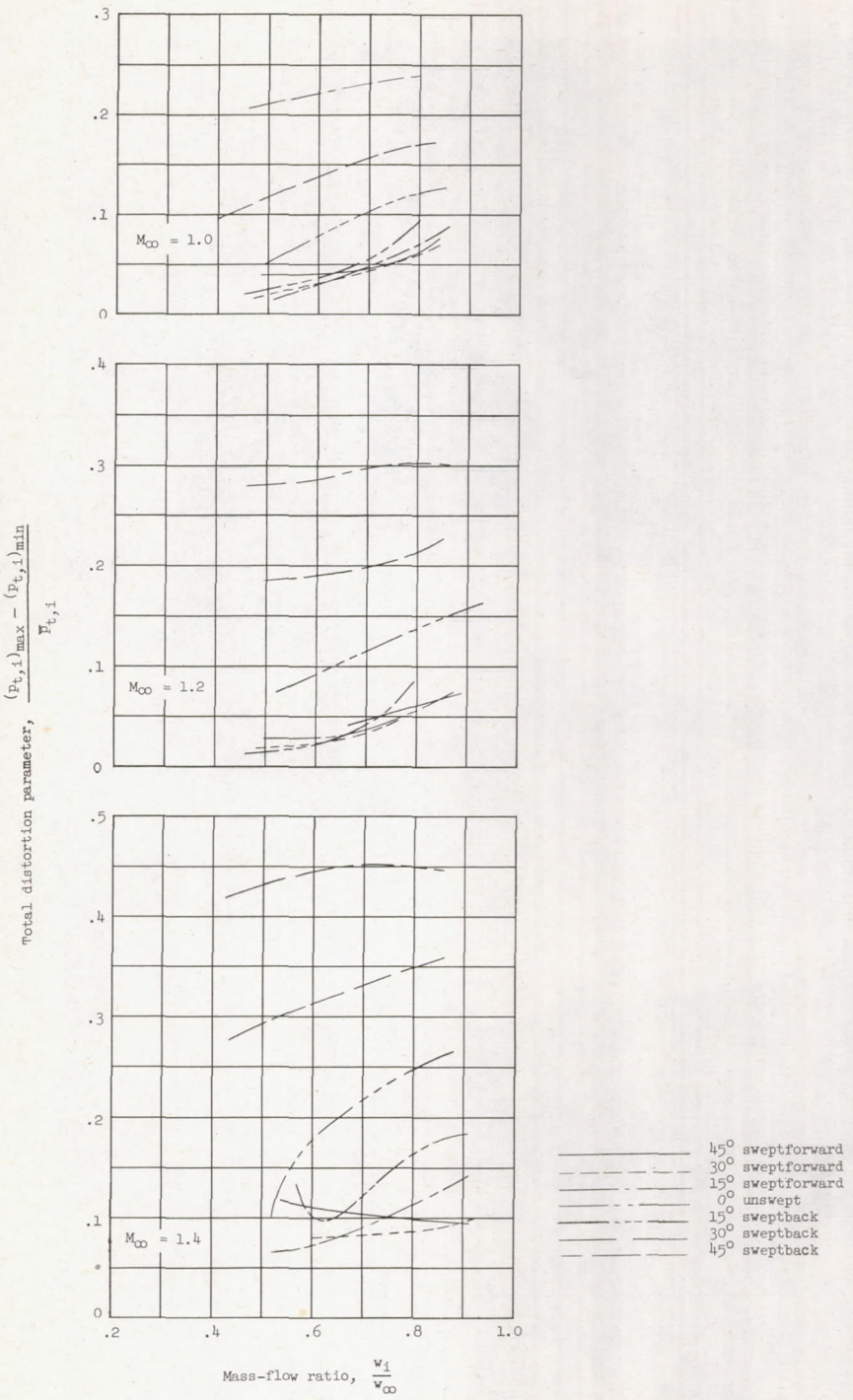

Figure 10.- Effect of variations in mass-flow ratio, Mach number, and lip sweep on the flow distortions at the inlet measuring station.

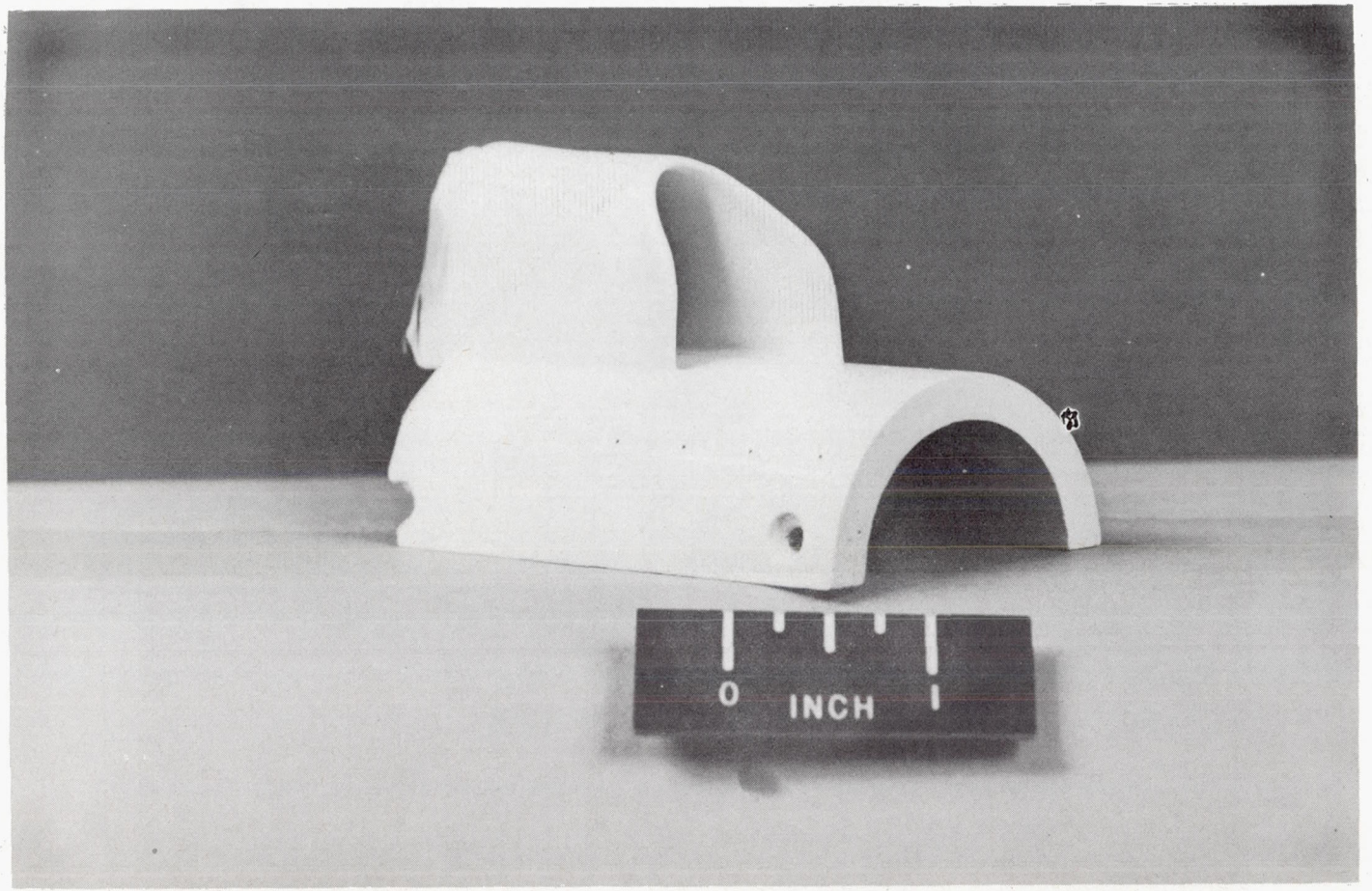

(a) 45° semiswept inlet model. L-89187

Figure 11.- Three-quarter front views of 45° semiswept inlet model and 45° sweptback inlet model with diverter.

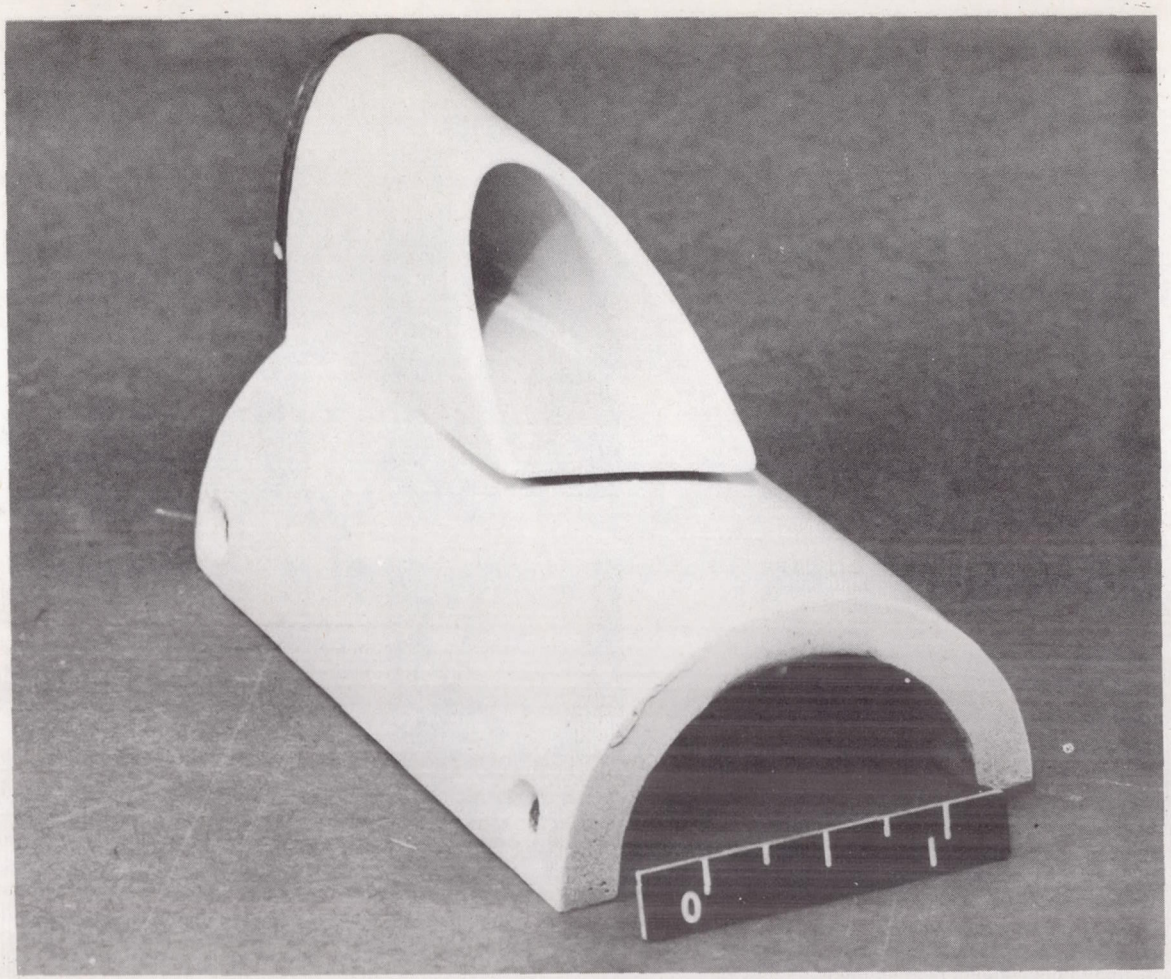

(b) 45° sweptback inlet model with diverter. L-89609

Figure 11.- Concluded.

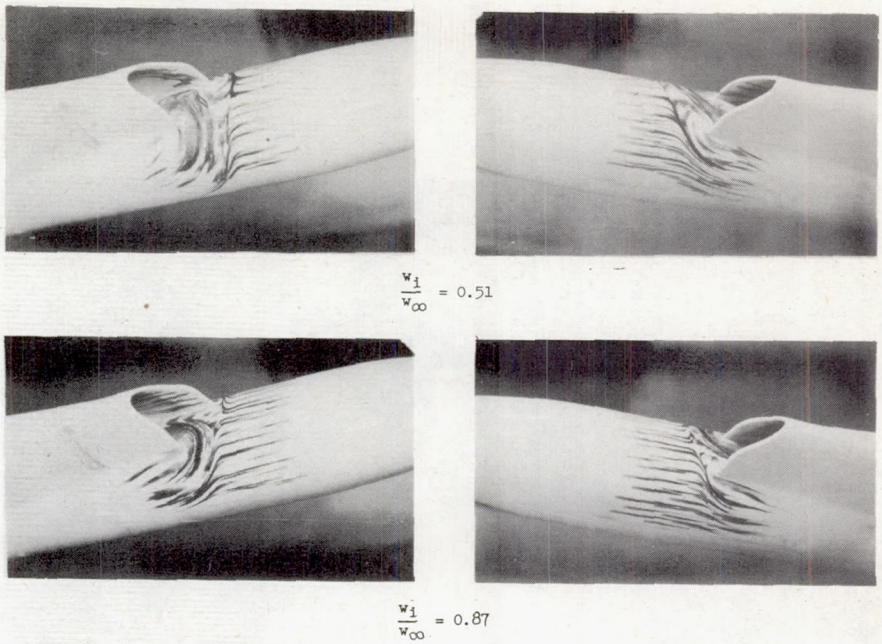

$\frac{w_i}{w_\infty} = 0.51$

$\frac{w_i}{w_\infty} = 0.87$

(a) 45° semiswept inlet.

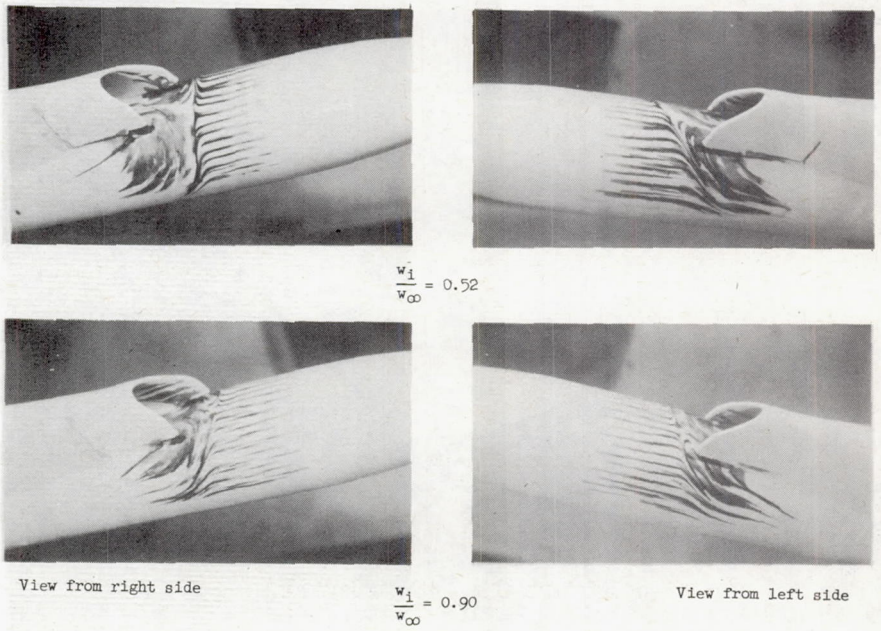

$\frac{w_i}{w_\infty} = 0.52$

$\frac{w_i}{w_\infty} = 0.90$

View from right side

View from left side

(b) Slotted 45° semiswept inlet. L-57-1582

Figure 12.- Oil-flow-study photographs indicating direction of boundary-layer flow at $M_\infty = 1.4$ for several modifications to the 45° swept-back inlet.

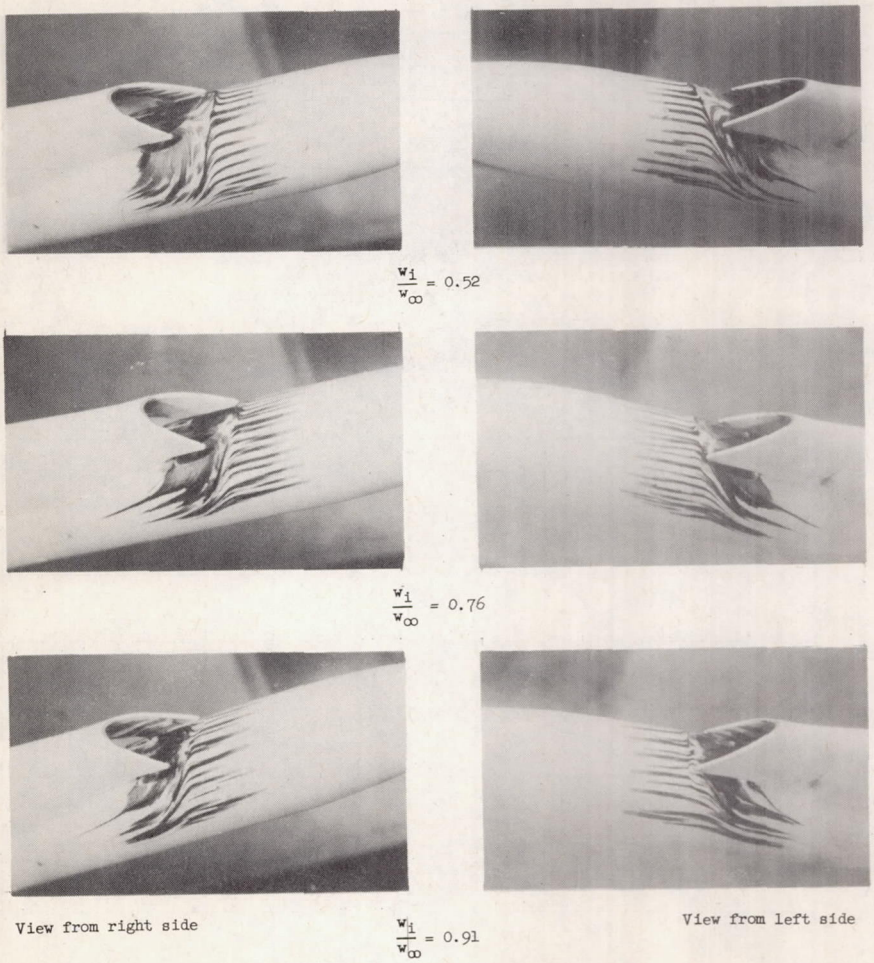

(c) Slotted 45° sweptback inlet. L-57-15

Figure 12.- Concluded.

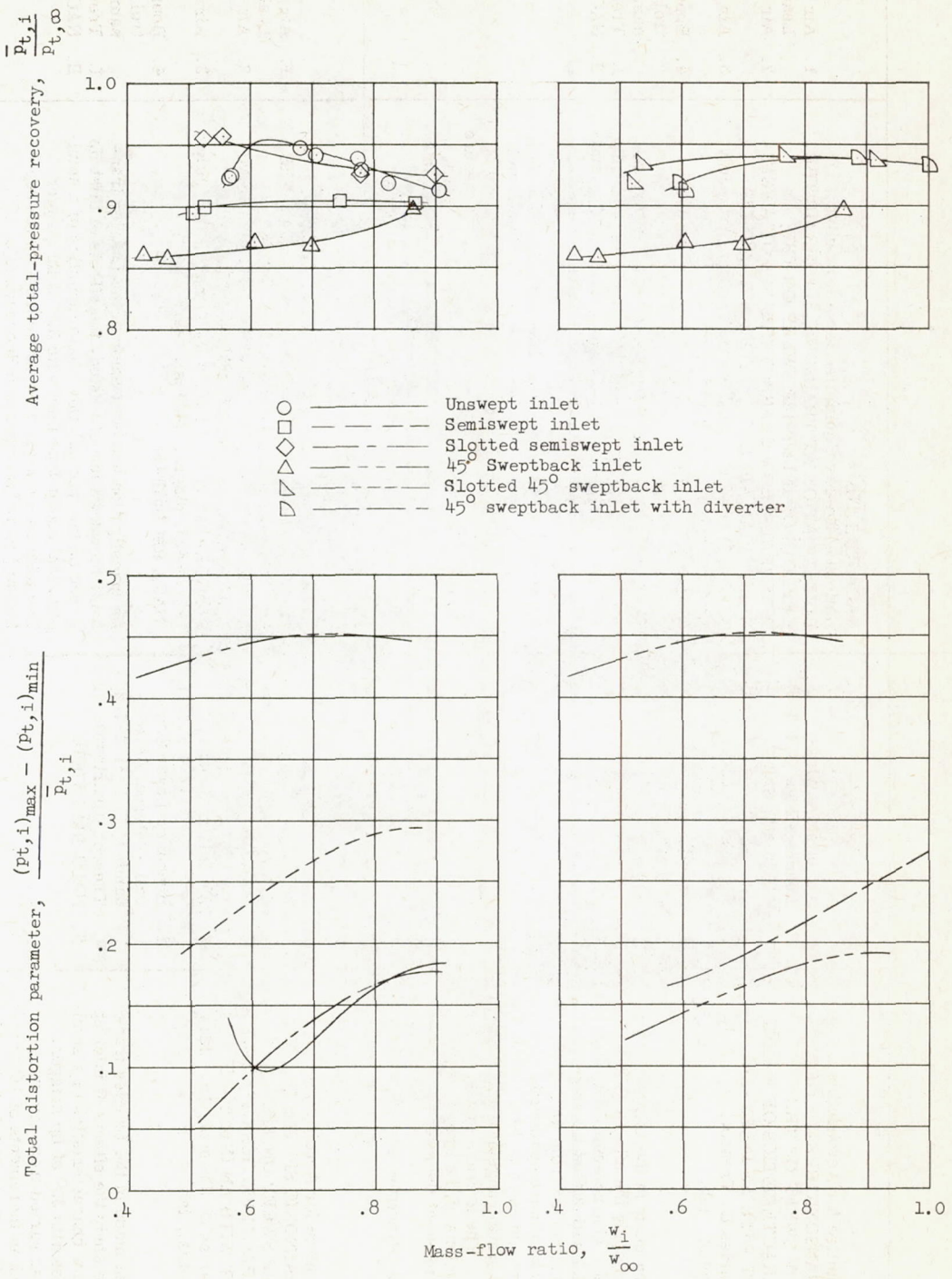

Figure 13.- Effects of several boundary-layer control devices on the total-pressure characteristics of a 45° sweptback inlet at a Mach number of 1.4.